Report 1 PHIN-CARE-JRA2-WP3 Second Task Pulse Shaping

I. Boscolo, S. Cialdi,* F. Castelli and D. Cipriani
University and INFN, via Celoria 16, 20133 Milano, Italy

December 2, 2005

Abstract

This report presents the activity developed on *laser pulse shaping argument* in years 2004-2005 by Milano-INFN within the framework of CARE /JRA2 "Charge production with Photo-injectors" second task "Pulse Shaping". A dedicated laser system with the relative diagnostic tools have been developed. A liquid crystal programmable spatial light modulator(LCP-SLM) shaper have been studied and set for the generation of different waveforms. The shaper is integrated in the laser system for an automatic generation of the target waveforms via the insetion of a computer which drives the system through the developed software. The system can be programmed to generate any target waveform compatible with the spectral bandwidth of the laser system and some exemples are presented. The following issues are treated: (i) the operation stability as function of perturbations of the set-up parameters, (ii) the design of the shaper for the SPARC project, (iii) a new shaper concept for the generation of long target waveforms and (iiii) the rectangular pulse generation at the second harmonic.

1 Introduction

High brilliance radiofrequency electron guns (rf-gun) are driven by UV laser pulses [1]. Experimental tests reported in Ref. [2] showed that the e-beam emittance depends on the temporal laser pulse characteristics and the emittance reached a minimum with a rectangular pulse. A subpicosecond Gaussian-like laser pulse is transformed into a rectangular one by a shaping system properly arranged. A typical laser system incorporating a shaper is shown in Fig. 1.
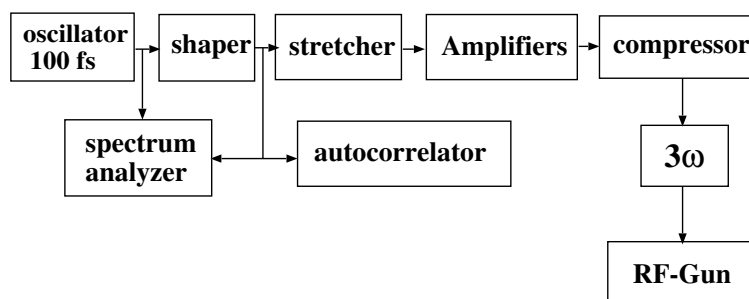

Figure 1: System layout with a pulse shaper insertion.

The technology for manipulating sub-picosecond pulses in order to generate ultrafast pulses according to user specifications has already been developed [3, 4]. We apply the basic ideas developed for narrowing laser pulses (from picosecond to femtosecond range) for generating relatively

---

*Electronic mail: simone.cialdi@mi.infn.it

long (around 10 picosecond) rectangular pulses with fast rise time (less than a picosecond). The principle of pulse shaping is based on the phase and amplitude modulation of the pulse spectral components. A rectangular pulse with a subpicosecond rise time can be obtained from a femtosecond laser pulse thanks to its high frequency content. However, the basic physics and properties of a shaping system capable of providing 10 ps rectangular pulses can be tested with a picosecond laser pulse, that is with a laser of the previous generation, therefore, not so much expensive. In the framework of developing shaping techniques for relatively long waveforms, we have designed and developed a common actively mode-locked Nd:YAG delivering pulses of 90 ps at 100 MHz with an average power of 5 W, followed by a 500 m monomodal optical fiber for broadening the spectral bandwidth of a factor higher than 100, passing from 0.02 to 3 nm. We have also developed the diagnostic tools, that is an autocorrelator and a spectrometer, for on-line pulse profile and spectrum measurements. The liquid crystal programmable spatial light modulator(LCP-SLM) shaper (also called 4f-system) [3] was selected for its capability to provide long laser pulses. It was configurated for phase modulation of the spectral components. This shaper and the diagnostic tools are connected to a computer in a feed-back loop for autoconsistent operation. This system configuration is compulsory because the powerful lasers used to drive rf-guns (most commonly, Ti:Sa lasers operating at the third harmonic [1]) are multi-component systems (with amplifiers and harmonic converters) having inherent configurational perturbations and therefore some instability in the output waveform. This instability connected to the shaper sensitivity to it leads quite naturally to set the entire laser system in a self-organized mode of operation towards the generation of a target output pulse as we have developed, see Fig. 2 .
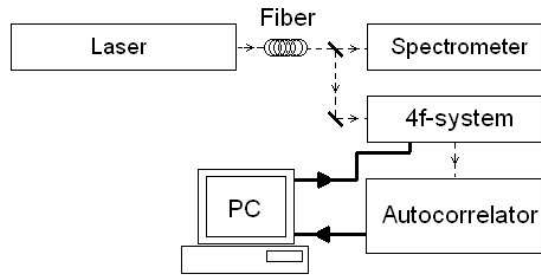

Figure 2: Schematic of the laser system complete of shaping system and the fundamental diagnostics.

This paper is organized in the follwing manner: (a) The first part treats the design and the tests of the system for the generation of pulses of rectangular, double-pulse and multi-pulse profiles; in succession are presented (b) the operation stability as function of perturbations of the set-up parameters, (c) the design of the shaper for the SPARC project, (d) a new shaper concept for the generation of long target waveforms and (e) the rectangular pulse generation at the second harmonic.

2   The Nd:YAG oscillator

The Nd:YAG oscillator has been designed for actively mode-locked operation at 100 MHz and single TEM_{00} transverse mode.
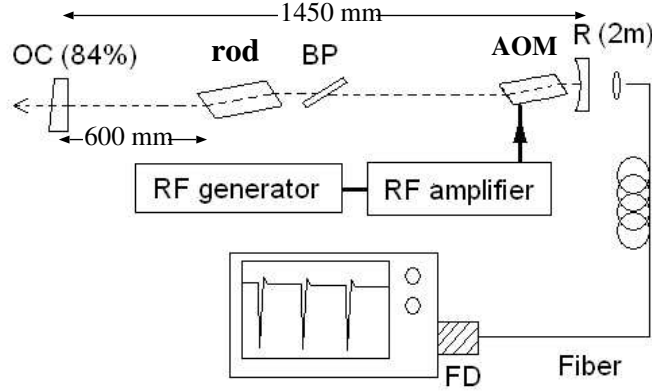

Figure 3: Schematic of Nd:YAG oscillator with its components: OC = Output Coupler, RM = Rear Mirror, BP = Beam Splitter.

The design of the cavity was done exploiting the matrix propagation of the light beam through the optical components. The constrains of 100 MHz frequency, fundamental TEM_{00} mode and an optimized trade-off between the output power and the pulse length guided the choices (shown in Fig. 3) of cavity length, laser rod position, radius of the rear reflector mirror and transmittance of the flat output coupler.
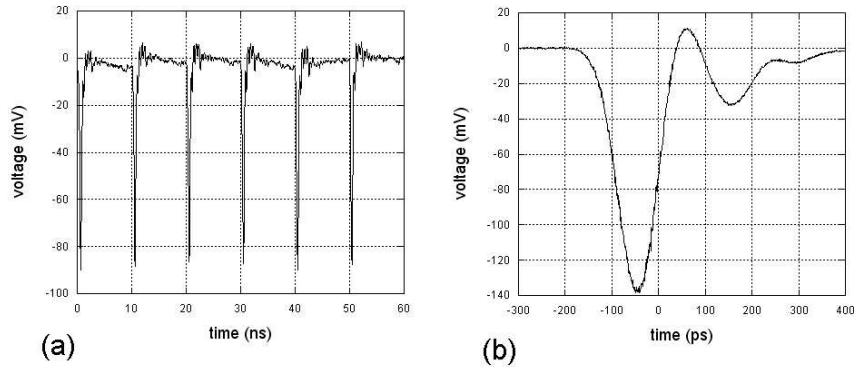

Figure 4: Output pulses: Frame a shows the train of pulses a good stability; Frame b shows the single pulse width (the overshoot at the end of the pulse is due to the pic-up monitor.

Fig. 4 shows the train and the single pulse shape detected by a 30 ps rise-time photodiode placed at the rear mirror. The depicted pulse has a length of 93 ps. The best observed result was 70 ps. This was obtained with fine tuning of AOM configuration (alignment along the three axis es, RF-tuning and high modulation), fine tuning of the cavity length (the output mirror is submicrometrically set) and fine alignment of the laser rod.

Bandwidth broadening by a 500 m optical fiber insertion

A guided optical wave propagating in a single mode fiber experiences a uniform self-phase modulation which broadens the spectrum. We have coupled the Nd:YAG laser to a 500 m long
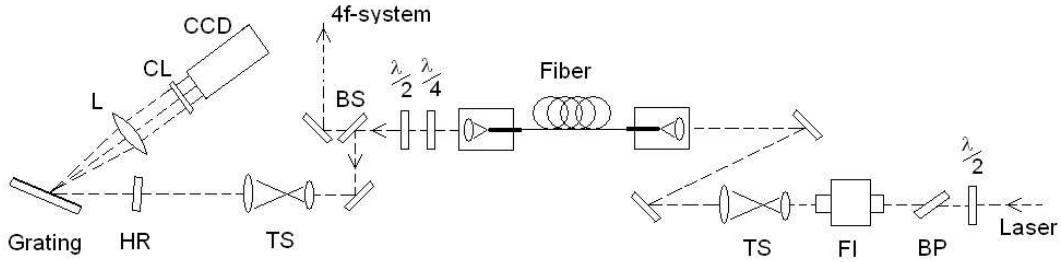
Figure 5: Scheme of the optical components and the fiber added to the laser oscillator for spectrum broadening. The spectrometer is also depicted.

single mode, polarization preserving optical fiber for extending the spectrum of our laser pulse from the initial 0.02 to a final 2 nm, see Fig. 5.

The equation governing the wave complex amplitude A

$$\frac{\partial A}{\partial z} = -\frac{1}{2}\,\alpha A - i\,\frac{1}{2}\,\beta\,\frac{\partial^2 A}{\partial^2 t} + i\,\frac{1}{L_{NL}}\,|A|^2\,A \tag{1}$$

with β the propagation constant (in our fiber $\beta = 17\,ps^2/km$) and α the the loss factor ($\alpha = 2.2\,dB/km$). The first term of the equation is the loss term, the second term is the dispersion term (the longer the wavelength the faster the wave runs) and the third term governs the self-phase modulation. The quantity L_{NL}, called non-linear length, signs the starting of the non-linear action. The spectrum broadening $\Delta\omega_{out}$ from Eq. 1 comes out to be

$$\Delta\omega_{out} = \frac{L_{fiber}}{L_{nl}}\Delta\omega_{in} \propto P\,L_{fiber}\,\Delta\omega_{in} \propto P_M \cdot \frac{\Delta T}{\Delta\tau}\,L_{fiber}\cdot\frac{1}{\Delta\tau} \tag{2}$$

where P_M is the average power, ΔT is the the round trip time (in our cavity 10 ns) e $\Delta\tau$ the pulse temporal length. Once given the laser pulse power and the fiber characteristics the spectrum broadening depends on the fiber length. Eq. (1) has been solved numerically by the split stop Fourier method and the output spectrum obtained for our laser beam and optical fiber parameters is shown in Fig. 6. As expected when the output pulse of the laser is Gaussian, the smoothed phase function has a parabolic shape (that one of chirped pulses). Superimposed to the parabola there is a small fast oscillation of the phase. This oscillation is in correspondence of the power spectrum oscillation as shown by the figure. Frame b of Fig. 6 shows the measured power spectrum and the relative power spectrum calculated taking into consideration the resolution of the spectrometer.

2.1 Oscillator operation with SESAM insertion

Aiming to enlarge the bandwith up to 8-10 nm for a subpicosecond pulse we did some tests on the oscillator with a semiconductor saturable modulator (SESAM). The best result was about 25 ps, as shown in Fig. 7. However, in the common operation the oscillator delivers a pulse of about 40 ps. The result is determined by the fact that the company does not produce the SESAM tailored to our laser.

2.2 The spectrum analyzer as powerful diagnostic tool

We have designed and built a spectrum analyzer tailored to the characteristics of our laser pulse, see Fig. 5: the grating of 1714 lines/mm is coupled to a lens of 400 mm focal length so to obtain a spatial dispersion of 0.68 nm/mm.
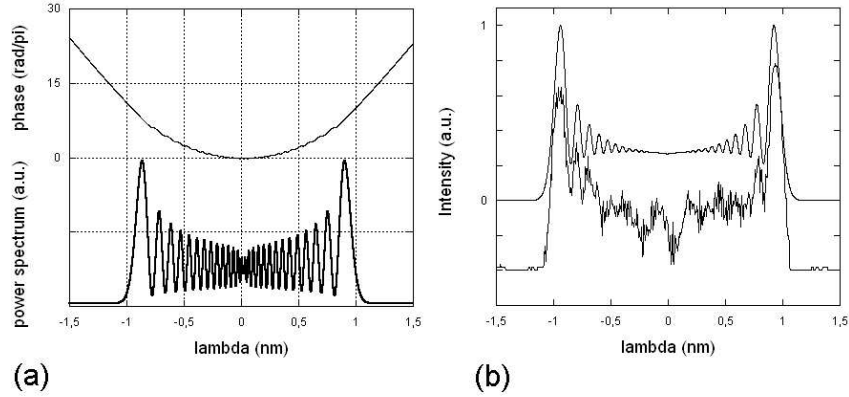
4

Figure 6: Frame a, simulated spectrum at the output of the optical fiber and the relative phase function. Frame b, the upper curve is again the simulated spectrum but convolved with a proper Gaussian curve, the power signal is the relative measured spectrum function.
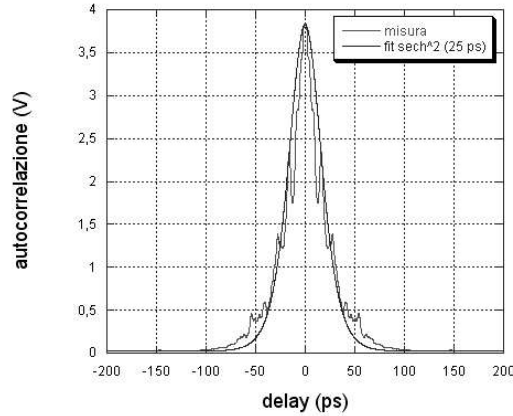

Figure 7: The autocorrelation pulse of the Nd:YAG oscillator after the insertion of a SESAM of

The linear enhancement of the spectrum bandwidth with the average laser power, as predicted by Eq.(2), is experimentally reproduced in Fig. 8, where the four spectra relative to 100-200-300-400 mW power are reported. In Frame b the variation of the spectrum which occurred within half an hour is depicted: it covers an interval amplitude of about 4 %.

We note that the spectrum recorder is fast, thus it is exploited for the measurement of the temporal pulse length and its profile because the spectrum characteristics are stricly related to the laser pulse characteristics.

3   The LCP-SLM shaping system

The operational principle of the system, the computer program developed for the simulations with its performance and the configuration for an autoconsistent operation are discussed. The main parameters are presented in Ref. [5].

The pulse shaping is a linear filtering process. In the time domain the filter action of the shaper is represented by an *impulse response function* $h(t)$, while in the frequency domain the filter action is represented by its Fourier transform $H(\omega)$. The output waveform $e_{out}(t)$ is the convolution of the input waveform $e_{in}(t)$ and the impulse response function h(t)
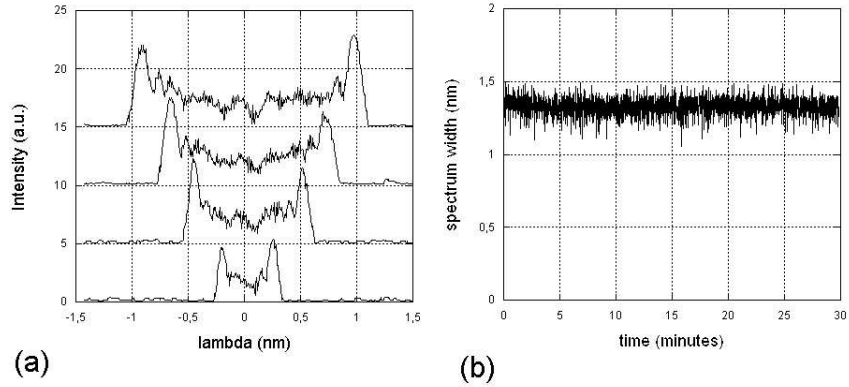
Figure 8: Frame a: set of measured spectra as function of the output average power, namely 100, 200, 300 and 400 mW respectively from bottom to top. Frame 2: jitter of the spectrum width in half an hour.

$$e_{out}(t) = h(t) * e_{in}(t) \tag{3}$$

In the frequency domain we may write

$$E_{out}(\omega) = H(\omega) \cdot E_{in}(\omega) \tag{4}$$

In general $H(\omega)$ will be a function of the type

$$H(\omega) = T(\omega) \cdot e^{-i\psi(\omega)} \tag{5}$$

Appropriate amplitude $T(\omega)$ and phase $\psi(\omega)$ modulations lead to any kind of output signal. However, in problems where the demand is limited to the temporal intensity profile only, as is the case of rf-guns, a phase-only modulation can be applied. In fact, the time domain intensity (and amplitude) is specified but the temporal phases are free.

3.1 Operations of the shaping system

The optical components of a 4f-setup are two gratings and two lenses placed at the focal distances with a filter mask placed at the center focus plane, as shown in Fig. 9. In this system the
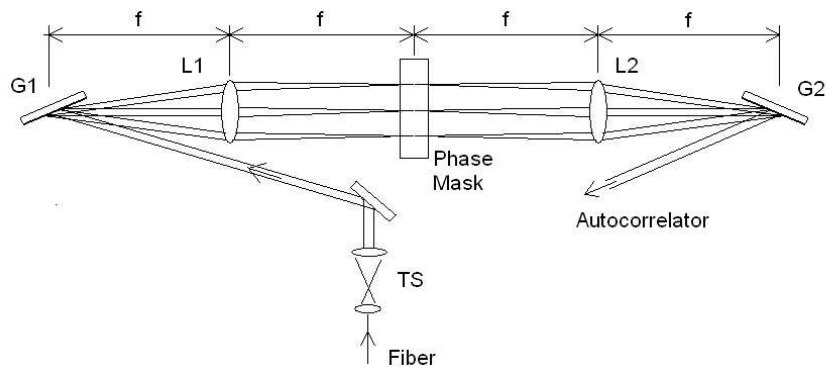

Figure 9: Scheme of the 4f-shaping system, top view. The light polarization lays on the plane of the figure (that is the plane of the optical table.

6

spatial dispersion is done by a simple lens-and-grating pair, the filtering is made by an array of liquid-crystal-spatial-light-modulators (LC-SLM), called in short mask, see Fig. 11, and the ray compnents are recombined by a second lens-and-grating pair. The system is called 4f-system because the five optical components are set at the focal distances one another (so to produce positive group velocity dispersion). There is a programmable acousto-optic modulator which can operate as dispersive filter (AOPDF) [4]. The mask is an array of rectangular pixels interlived by small transparent gaps.The task of the mask is to introduce definite phase retardations (or amplitude mosultions) onto the spectral components. We analyze and discuss the experimental results of the mask as phase-filter. The output waveform is determined by the patterned phase function set at the mask in conjunction with the dispersion strength (i.e. the dimension of the 4f-system) of the grating-lens apparatus. We analyze the behavior of the 4f-system with the purpose of finding the limits of the operation for getting a shaped waveform with good fidelity.

The temporal resolution of the shaped waveform is limited by the bandwidth of the input pulse and the spatial resolution of the mask limits the temporal range of the shaped waveforms.
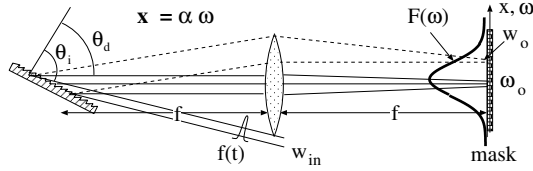

Figure 10: The input θ_i and diffracted θ_d angles by the grating of 4f-system. The mask and the grating are placed at the distance f from the lens. The Gaussian Fourier spectrum is depicted at the mask. The spectral components of the input light beam are separated by the grating and focused at the mask by a lens with a beam waist w_0.
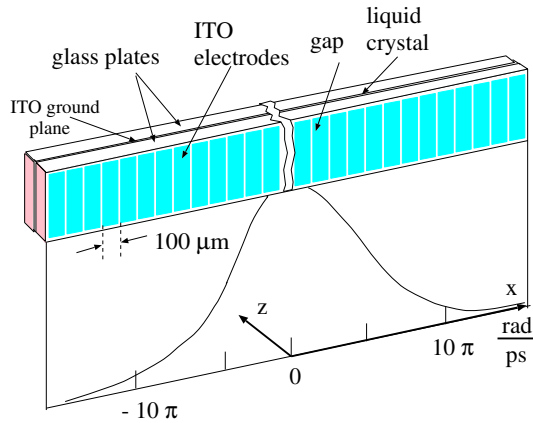

Figure 11: Schematic diagram of an electronically addressed LCP-SLM. A thin layer of nematic liquid crystal is sandwiched between two peaces of glass. The inside surface of each piece of glass is coated with a thin, transparent conducting film of indium tin oxide patterned as an array of pixels.

The mask of an LCP-SLM system is an array of pixels interleaved with small gaps, see Fig. 11. The chosen mask is the Jenoptik model SLM-S 640/12 mask (JENOPTIK Laser, Optik, System GmbH, Jena, Germany). The dimensions of the pixels and gaps are respectively $97\,\mu m$ and $3\,\mu m$ wide and the number of pixels is 640.

The spectral dispersion follows, in first approximation, a linear law

$$x \simeq \alpha\omega \qquad (6)$$

7

The frequency ω is referred to the central frequency ω_0 of the spectral domain spanned by the signal. The filter function $H(\omega)$ is related to the physical transmission function of the mask. We observe that the field just after the mask, calling $H_{SLM}(x)$ the physical transmittance of the mask, is given by

$$E_{out}(x,\omega) \sim H_{SLM}(x)\, e^{-\frac{(x-\alpha\omega)^2}{w_0^2}}\, E_{in}(\omega) \tag{7}$$

3.2 Configuration of the 4f-system

The configuration of the 4f-system is determined by the grating law and the equation of the beam waist w_0 at the mask pixel [5]

$$\lambda = d(sin\,\theta_i + sin\,\theta_d) \tag{8}$$

$$w_0 = \frac{cos\,\theta_i}{cos\,\theta_d} \cdot \frac{\lambda\,f}{\pi\,w_i} \tag{9}$$

In the above equations f is the focal length, λ is the wavelength, θ_d and θ_i are the diffracted and incident angles of the central frequency respectively (see Fig. 10) and w_i is the input beam waist at the grating.

The guidelines for the 4f-system configuration design are: (i) the spectral dispersion should be maximized so to exploit the maximum number of mask pixels and (ii) the beam waist at the pixel must be smaller-equal to the 100 μm pixel dimension. Since the larger the dispersion the larger is the waist at the mask, the best trade-off must be found. We note also that the waist at the mask w_0 is inversely proportional to the waist w_i at the grating.

In our system we ended up to the following parameters: gratings with 1740 lines/mm, achromatic lenses of 50 cm focal length, 65° degree input angle, $w_i = 2.3\ mm$ and $w_0 \leq 100\ \mu m$. In this configuration each nm of spectrum bandwidth covers 27 pixels of our mask.

3.3 The driving of the mask

The mask pattern configuration (filter function) is set by a computer through a serial gate. A voltage applied to the electrodes sandwiching the liquid crystal of a pixel drives the crystal orientation. The voltage ranges in the interval 0-8 V with a step resolution of 12 bit (corresponding to 4096 possible voltage values). The principal axis of the crystal lays on the table plane x-z. This decides the polarization of the light coming from the grating for the highest efficiency.

The mask must be calibrated before starting the operation. This calibration operation is done putting, in front of the mask, an amplitude modulator whose transmittance T depends on the voltage applied to the pixel. In this way we can build the curve T versus V. The amplitude modulator arranged in the Lab was made by a simple half-wave-plate set in front of the mask which rotates the polarization of 45° and a polarizer set in the back of the mask at 90° with respect the input polarization of the light. The transmittance T is given by

$$T = sin^2\left(\frac{\Delta\phi}{2}\right) \tag{10}$$

thus

$$\Delta\phi = \frac{2\pi\,d}{\lambda}\left[n_e(V) - n_0\right] \tag{11}$$

The curve of the voltage, that is of the corresponding number, versus the phase modulation obtained with the apparatus is shown in Fig. 12. From the curve we get that the maximum de-phase on a spectral component (for our 1064 nm radiation) is higher than 2π but minor than 4π.

It is wise to select a zone of 2π variation and possibly linear. Therefore, we chose the interval 0.5-2.5 rad/π. This means that we have 300 possible voltage values. We did the fit which transforms the voltage number into the phase modulation.
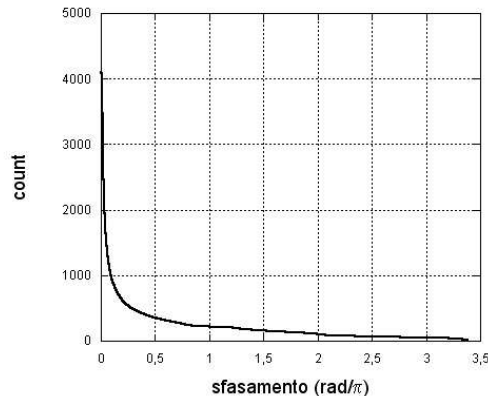
Figure 12: Curve of pixel voltage versus phase variation obtained in the calibration process.

4 The autocorrelator for the pulse profile measurement

The common tool for the laser pulse profile measurement is a cross correlator. But this technique can be used only in conjunction with a laser pulse much narrower than the pulse to be diagnosed. Our laser does not allow to exploit that technique owing to its long output pulse. Therefore we have built an autocorrelator for the measurement. We are aware that there is not a strict correspondence between the autocorrelation pulse and the temporal pulse. However, the profile of the pulse can be derived from the autocorrelation output for a certain class of pulses as Gaussian, rectangular, multi-Gaussian, and others. Since these are the pulses of our interest, an autocorrelator can be positively considered. For completeness, we are developing a numerical code, as PICASO [6], capable of producing the temporal pulse profile from the autocorrelation and spectrum signals.

5 A feedback arrangement of the shaping system for automatic operation

An analytical calculation of the response function H_{SLM} does not exist, it is found by a numerical calculation via an adaptive algorithm. The solution is implemented in the laser system by a proper setting of the shaping system. A computer, running the adaptive algorithm, can drive the system towards the right optical configuration of the mask.

The appropriate modulation (phase) function is calculated with an iterative procedure: the spectral patterned function is updated according to a Genetic stochastic optimization Algorithm (GA) [7]; a $cost-function$ C is calculated with the new signal obtained from the autocorrelator after the application at the mask of a fase function

$$C = \int |A_{target}(\tau) - A_{measured}(\tau)| \, d\tau \quad ; \tag{12}$$

if the $cost-function$ results minor than the best $cost-function$ found in previous cycles, the updated spectral patterned function is accepted, otherwise it is rejected and a new cycle starts with a fresh spectral pattern function. The iterations are stopped when the value of the $cost-function$ arrives to saturation. The final phase pattern is transferred to the mask. The complex spectral field $E(\omega)$ of the input pulse, that is its spectral amplitude $A(\omega)$ and phase $\Phi(\omega)$) and the temporal amplitude $E_{target}(t)$ of the target pulse are given as inputs. The calculation procedure is illustrated in Fig. 13. The initial trial phase vector Φ has all the phases at the pixels set at zero value and the value of the cost function is fixed very high.
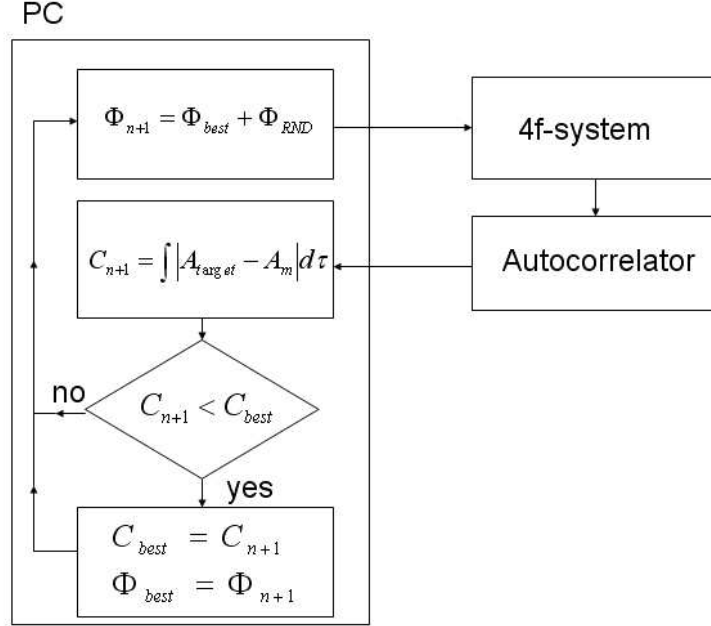
Figure 13: Flow chart of the numerical program for the simulation of the calculation of the phase function .

We have followed two different numerical approaches. In one the phase function is written as a power expansion

$$\Phi_{rnd}(\omega) = a_{rnd}\,\omega^2 + b_{rnd}\,\omega^3 + c_{rnd}\,\omega^4 + \ldots \quad , \tag{13}$$

The adaptive algorithm searches for the appropriate phase filter function varying randomly the coefficients of the expansion and applying the iterative calculation up to the achievement of the best target profile [7]. In the second numerical approach the phase function is written as the sum of a function counter-fitting the main component of the curve representing the phase function of the imput signal and a spectral patterned randomly searched function $\delta\psi_{RND}(\omega)$

$$\Phi(\omega) = f(\omega) + \delta\psi_{RND}(\omega). \tag{14}$$

In each iteration a random phase change $\delta\psi_i$ is generated according to $\delta\psi_i = R$ where R is a random variable uniformly distributed in a definite interval. The index i refers to the i-th pixel. This second approach for our case of input pulse after the optical fiber, means that the function $f(\omega)$ is a parabola, that is the phase function will be

$$\Phi(\omega) = \frac{1}{2}\alpha_{rnd}\,\omega^2 + \delta\psi_{RND}(\omega). \tag{15}$$

The parabola counter-acts the parabolic phase generated by the self phase modulation effect within the optical fiber.

The first procedure does not give a positive result when the phase profile of the output pulse is complex. In fact, a phase function with fast oscillations requires many terms in the power development (13). The same consideration holds transform limited input pulses.

The succession of operations occurring in the system in each iteration are: a random variation of the phase function (by a computer), its application to the mask, re-orientation of the mask pixels (in about half a second) and a consequent generation of a new (varied) output pulse, measurement of the autocorrelation signal (the computer starts to acquire from the autocorrelator the formed signal after 0.5 s from the releasing of the phase function), acquisition and renormalization (to

10

unity) of its area, comparison of the signal with the target one via the cost-function and a new cycle starts.

6 Results and discussion

In this section we discuss the generation of four different waveforms shaped having as input pulse the chirped Gaussian-like pulse of about 110 ps provided by our laser system (oscillator and optical fiber). The system arrangement for the pulse modulation had to take into consideration a notable diffraction effect observed when the velocity of variation of the phase introduced for obtaining a new waveform was higher than a certain value. This effect is, therefore, treated in the next subsection in connection with the discussion of the first searched waveform. In our laser system we have to compare the autocorrelated target pulse with the autocorrelated output pulse from the 4f-system (instead of the direct temporal pulse).

6.1 Pulse compression to 2 ps length and the diffraction problem by the mask

The input pulse can be compressed setting a parabolic phase function to the mask which counteracts the phase modulation introduced by the fiber. The pulse, as shown in Fig. 14 Frame a, is compressed from the initial 110 ps to few ps. Frame b shows the phase function that the computer sent to the mask. The parabolic function is many-folded in order to maintain the phase variation among the pixels within the interval $-\pi \div +\pi$. The values of the phase function are converted in numbers that are sent to the mask. The replica pulses due to the patterned configuration of the
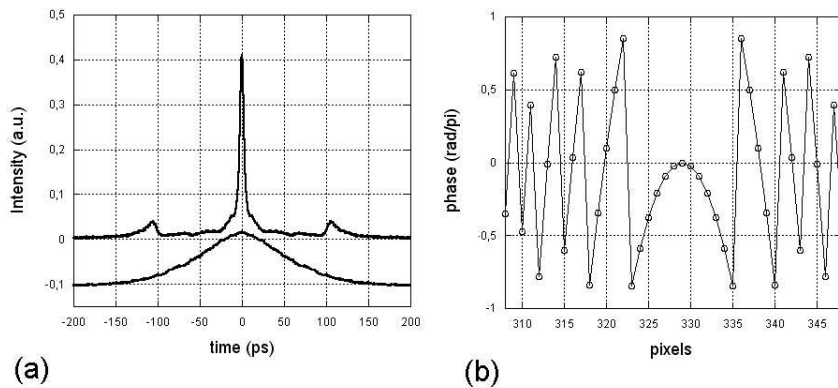

Figure 14: Frame a: the lower trace is the input 100 ps pulse and the upper trace is the 3 ps compressed pulse by the 4f-system; Frame b shows the phase function at the mask pixel.

mask with pixels interlived with gaps are eliminated by the proper choice of the waist dimension onto the mask pixel [5].// Remarkably, the output signal has two evident side pulses at a distance of about 100 ps from the main pulse. These pulses come out to be due to the fast slope of the parabolic phase curve (at the sides) necessary for the strong compression, which, in turn, means a large phase variation between two adjacent pixels. The effect is amplified by increasing the slope. We have observed on a screen set just at the back of the mask, in fact, the appearance of two bright spots at the sides of the central spot starting from a certain slope. Looking at the position of the spots in relation to the phase curve, see Fig.15, we could see the correspondence between the bright spot and the smooth phase variation and, complementary, the dark place and the strong phase variation between the pixels.

Systematic observations lead to find the following empirical limit of the phase variation between two adjacent pixels
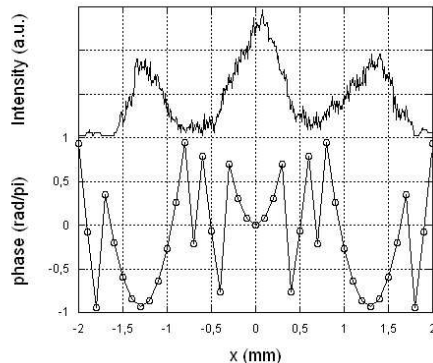
Figure 15: Intensity of the output signal obtained at a screen placed at 7 cm from the mask, upper trace, and the corresponding phase function, lower signal.
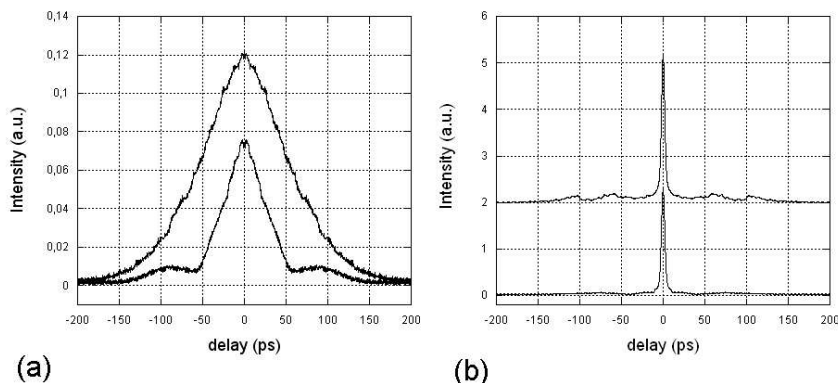

Figure 16: Frame a: the upper and the lower autocorrelation traces of the input pulse respectively without the iris in front of the mask (the laser pulse) and with the iris. Frame b: the two corresponding pulses compressed by the shaping system. The compressed pulse obtained with the iris insertion is much more neat.

$$\frac{\Delta\phi_{max}}{\Delta\omega_{pixel}} = \frac{\pi/3}{\delta\omega_{pixel}}. \tag{16}$$

in order to avoid the diffraction action (remembering that the delay time between the frequency ω and the central frequency ω_0 is: $\tau(\omega) = \partial\phi(\omega)/\partial\omega$). This condition gives the maximum compression $\Delta\tau_{max}$ that can be obtained without meeting pulse deformation due to diffraction. In our system the maximum compressible pulse length comes out to be 40 ps. The check was done reducing the pulse length simply cutting the wings of the pulse at the mask site with an iris and then compressing that pulse. The result is shown in Fig. 16. The two 100 ps and 40 ps pulses after compression are compared in Frame b: the second pulse is much more neat compared with the other. This mask behavior limits the shaping possibility because only a limited spectrum bandwidth is accepted with a pulse of that length. Therefore, the diffraction effect of the mask limits the rise time of a target rectangular profile.

12

6.2 A rectangular profile

The autocorrelation signal of a rectangular pulse has a triangular profile. The target pulse to be built was a rectangular one of 10 ps length. In this case the power expansion procedure requires only the second and the forth terms because of the parabolic profile of our input phase function. In Fig. 17 the two autocorrelation pulses, the target and the experimental one, are reported. In Frame b the cost function behavior with the number of iterations is reported. The two target and experimental signals overlap quite well, and the result is obtained in only 30 iterations. The rise time is about 3 ps because of the relatively narrow spectral bandwidth.

We would remark the good result with a relatively fast convergence in spite of the particular form of the input signal. In the most common case of a transform limited pulse (obtained for instance from a Ti:Sa laser) the number of necessary terms for obtaining a rectangular pulse would be not more than eight. Fig. 18 shows the result obtained applying the second procedure: the
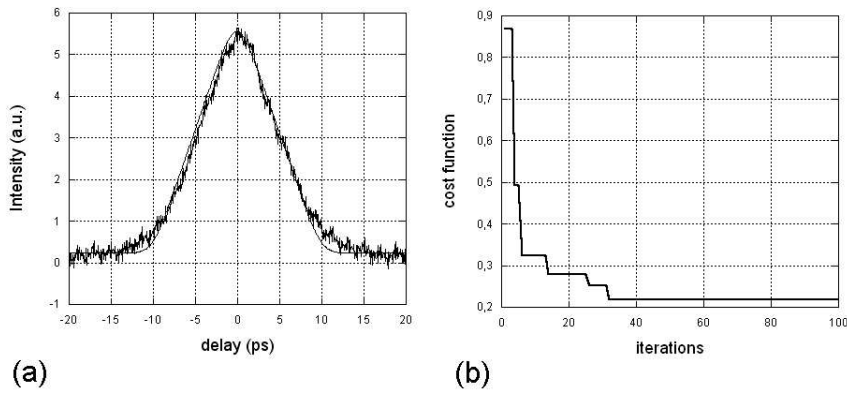

Figure 17: Frame a: the two target and measured autocorrelation signals of the rectangular pulse; Frame b: the number of iterations required for obtaining the final signal.
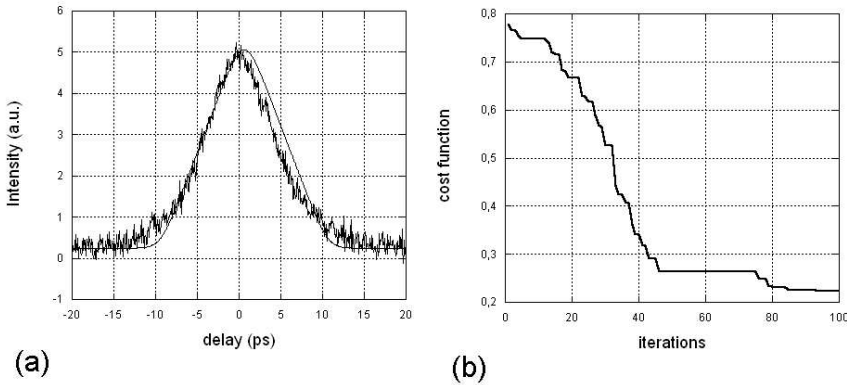

Figure 18: As previous Fig. 17 but the numerical simulation followed the second procedure. Frame a: the two target and measured autocorrelation signals of the rectangular pulse; Frame b: the number of iterations required for obtaining the final signal.

two signals do not match as in the previous operation and the number of iterations required is about a factor three higher. This is explained by the different calculation procedure: in the previous procedure only two coefficients were varied randomly, while in the second procedure all the phases of a patterned function relative to the array of pixels had to vary randomly. Moreover,

13

the very good fit obtained in the first procedure was due to the peculiar spectral function after the interaction within the fiber.

6.3   A double-pulse profile

The generation of a pair of pulses (pump-probe pulses) is another result interesting for several applications. The target pulse is a pair of pulses of 4 ps width and 12 ps interdistance. The result is shown in Fig.19. Again the output pulse reproduces quite well the target pulse. The proper procedure for this case was the second one and the number of iterations was higher than the previous case. Two remarks are worth doing: one is that the initial value of the cost-function was set at a much lower level than in the previous cases and the second one is that there is a proper temporal window for the integral of the cost-function. The initial low value of the cost-function is due to the relatively large width of the autocorrelation target pulse (not far from that of the input pulse). The temporal interval of integration cannot be too large because the integral would be affected by the numeral noise and would lead to a low value of the cost-function. It cannot be too short, on the other side, because the information on the shape of the whole pulse would be lost.

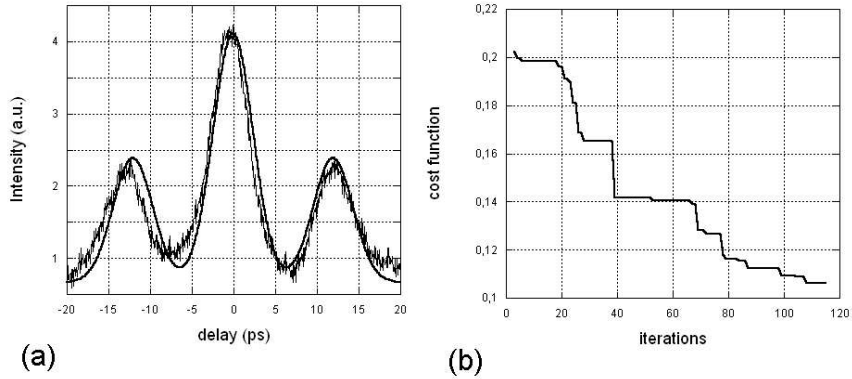(a)   (b)

Figure 19: Frame a: the two target and measured autocorrelation signals of a double pulse profiles; Frame b: the number of iterations required for obtaining the final signal.

6.4   A multi-pulse profile

The spectral filtering technique can be used for generating high-repetition-rate pulse trains. A pulse shape is the Fourier transform of the pattern transferred by the spatial filter onto the spectrum [8]. In our approach we use a spectral phase filtering: the phase response of the mask (filter) varies periodically with frequency, see Fig. 20. In this way the spectral bandwidth is divided in N sub-bandwidths whose distance in frequency is ΔF. Each radiation sub-bandwidth is conveyed into the relative pixel sub-array and will apply the same phase modulation. The repetition rate of the train is the frequency periodicity ΔF. The output intensity profile $I(t)$ is related to the input waveform $E(\omega)$ as

$$I(t) = \left(\frac{1}{2\pi}\right)^2 \int e^{i\,\omega\,t} d\omega \int E^*(\omega')\, E(\omega' - \omega)\, d\omega' \tag{17}$$

The intensity is the Fourier transform of the autocorrelation of the filtered spectrum. To obtain a set of pulses under a smooth envelope by using a phase filter, we must make a phase response with an autocorrelation that consists of a train of spectral peaks. Various pseudorandom phase sequences can provide this sequence.

The pixel were grouped in bunches of 5. The phase mask consisted of the repetition of the sequence
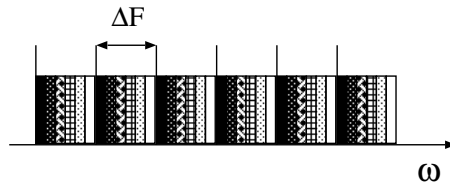
Figure 20: Generation of a pulse train by a phase spectral filtering. The various shaded rectangles denote the pixels with different phases.

[10010] where the logic 1 corresponded to $\Delta\phi = 0.7\pi$. The phase mask is sufficiently wide to pass the entire input bandwidth; consequently, the pulses in the shaped train are as short as the input pulses, $\simeq 3ps$ FWHM. Figure 21 shows the auto-correlation measurement of of the pulse train.
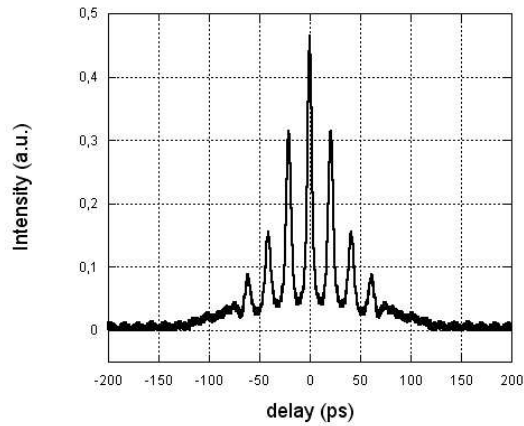

Figure 21: Auto-correlation measurement of the pulse train produced by phase periodical filtering.

7 System sentivity to perturbations of the parameters

We report here the paragraph 4 of the article "Features of a phase-only shaper set for a long rectangular pulse" J.Opt.Soc.Am. **21**, 1693 (2004).

We present now the variations on the output signals brought about by the deviations of the input signal parameters, that is pulse length, beam alignment, beam shape and finally mask position. The simulations are done applying to the different cases the spectral patterned function $\Phi(\omega)$ found for the reference input pulse (100 fs and Gaussian shape) and reference shaper parameters $w_0 = 20\,\mu m$ and centered light beam at the mask. The shift of the central frequency (due to a possible laser instability) is roughly equivalent to the shift of the mask along the x-axis direction. The results of the simulation, depicted in Figs. 22 and 23, are here listed.
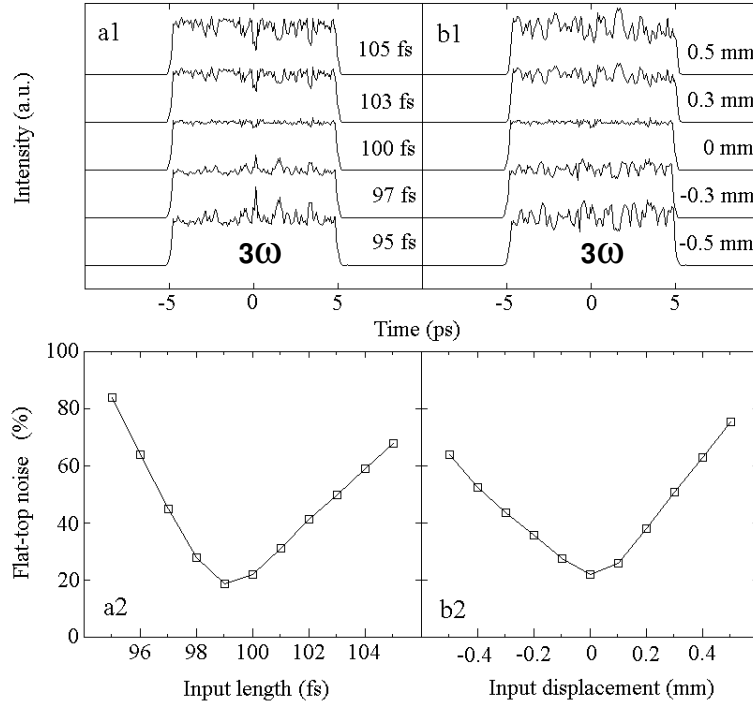
Figure 22: a1, b1, Variation of the output pulse (calculated after the conversion to the third harmonic) versus the variation of the pulse length, and b1, and shift from the centered position of the mask, right frame. a2, b2 Relative behavior of the the spiking amplitude over the mean value, i.e. $(I_{max} - I_{min})/I_{average}$, as function of deviations in the length and in the position of the mask.

Figure 23: Left and right, output pulses for the fundamental and the third harmonics, respectively, assuming a hyperbolic secant function instead of a Gaussian function for the input pulse. In the signals, we may say that the flatness is practically lost.

16

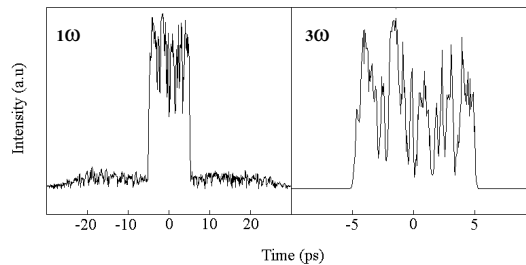- *Pulse length deviation of 5 fs.* If the pulse length changes down to 95 or up to 105 fs, the spiking amplitude $(I_{max} - I_{min})/I_{average}$ on the third harmonic at the flat top increases from 20 % to $\sim$ 80 %.

- *Shift of the mask of 0.5 mm with respect the central position.* The spiking enhancement arrives up to $\sim$ 70 %.

- *Shift of the incident angle θ_i.* Since a variation of θ_i induces a variation on α (because of the grating action the spatial dispersion α depends on the diffracted angle θ_d, which in turn is a function of θ_i, i.e. $\alpha \propto 1/cos\,\theta_d(\theta_i)$ [3]) the spectral bandwidth hitting the mask is changed. This can easily seen looking at the expression of the spectral intensity at the mask

$$I(x) = e^{-\frac{\tau^2}{2\cdot(1.177)^2}\cdot\frac{x^2}{\alpha^2}} \tag{18}$$

where τ is the time pulse width. A small variation of α about the reference value induces a variation on the spectral intensity $I(x)$ analogous to that induced by the variation of the pulse length τ. Therefore, the previously seen results relative to the pulse length deviation can be extended to the case of θ_i small deviation: The 30 % spiking enhancement means a 2 % α variation.

- *Change of the input pulse shape.* In passing from the Gaussian shape to the hyperbolic secant shape (as possible for a mode locked oscillator) the reduction of the flatness is dramatic, see Fig. 23.
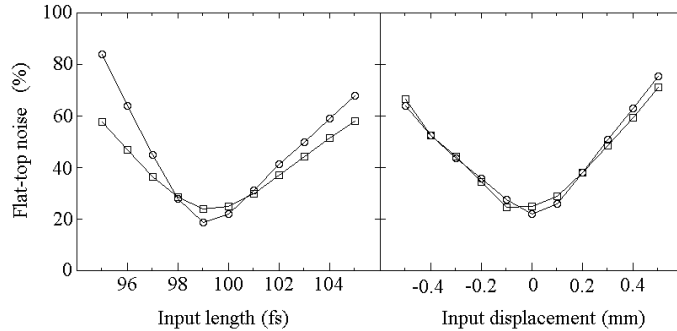

Figure 24: Left, variation of the plateau's flatness with the perturbation of the pulse length for the reference $30\,\pi$ rad/ps through the mask (curves with circles) and for a reduced acceptance of 3/4 of that reference acceptance (curves with squares). The latter is less sensitive to the perturbation. The curves at the right refer to the perturbations of the mask position. No sensible change occurs

Some comments are in order. The sensitivity of the shaper to perturbations, see Fig. 24, is related to both the phase-only filtering and the wide spectral acceptance. In fact, we have checked that the wider is the spectral acceptance the smoother the pulse flatness but also the higher the system sensitivity to any variation. It could be devisable for a lowering of the sensitivity to pulse length deviations to choose a less portion of the spectral bandwidth accepting a bit worse flatness . The spectral components relative to the signal tails turn out to be effective for smoothing down the roughness of the pulse plateau but the configuration of the spectral phases results so strict that a perturbation leads to a substantial pulse deformation.
The strong variation of the output signal with the change of the input signal profile comes as consequence of the relatively high variation of the amplitude of the spectral components. To reduce the sensitivity, an amplitude modulation besides a phase modulation should be applied.

8 The LC-SLM project for SPARC

We report here the paragraph 3 of the article "A laser pulse shaper for low-emittance radiofrequency SPARC electron gun" Nucl. Instrum. Meth. Phys. Res. A 526 (2004) 239.

The system configuration is largely determined by the angular dispersion α of the spectral components and is related to the system parameters by

$$\alpha = \frac{\lambda_0^2 \, f}{d \, 2\pi \, c \, cos[\theta_d(\lambda_0)]} \tag{19}$$

In the above equation f is the focal length, λ the wavelength, c the speed of light, θ_d the diffracted angle of the central frequency (Fig. 10). The equation comes from the grating law $m\lambda = d(sin\,\theta_i + sin\,\theta_d)$ with m=1. As we want efficient diffraction into the first order, for good spectral separation the grating period d should be as small as possible. The grating presented in brochures as having 2000 grooves/mm ($d = 0.5\,\mu m$) can provide the required dispersion of a few centimeters, at a distance of about half a meter for a 100-fs pulse with a carrier wavelength of 800 nm.
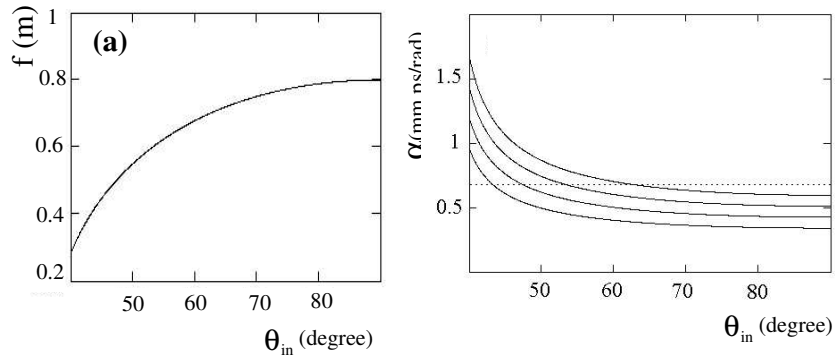

Figure 25: (a) Curve of the focal length as a function of the incident angle. (b) Angular deviation as a function of the incident angle θ_i for different focal lengths (in order from the top 700, 600, 500 and 400 mm). A trade off between θ_i and f must be done: the longer the focal length the lower the sensitivity to θ_i perturbation. As low sensitivity is needed, θ_i must be greater than 50°. The dotted line in (b) represents the possible incident angles for α slowly varying with angle.

The dispersion α remains fixed by the mask dimension Δx and the spectral bandwidth $\Delta\omega$ selected for the system, since $\alpha = \Delta x/\Delta\omega$. With the selected spectral portion of $\Delta\omega = 30\,\pi$ rad/ps we get $\alpha = 0.68\,mm \cdot ps/rad$. Once α is fixed, Eq. (19) relates the focal length to the input angle (Fig.25a). We looked at the variation in α with θ_i, (Fig. 25 b), to get a trade-off between the focal length and the input angle, so as to have a sufficiently low sensitivity of α to θ_i perturbations, combined with reasonable apparatus dimensions (that is a focal length). We propose a focal length $f = 700\,mm$ and, consequently, an input angle $\theta_i = 62.76^o$.

Mask and beam waist. The response function from Eq. (7), taking into account the finite number of pixels and the finite dimensions of the beam waist w_0, is

$$H(\omega) = \sqrt{\frac{2\alpha^2}{\pi\, w_0^2}} \, H_{SLM}(\omega) * e^{-2\frac{\alpha^2}{w_0^2}\omega^2} \tag{20}$$

We have already seen that the filter function $H_{SLM}(\omega)$ is step-shaped. The steps are smoothed by convolution with the Gaussian envelope function $e^{-2\alpha^2\omega^2/w_0^2}$ originated by the Gaussian spot of each spectral component at the mask. To conserve good spectral resolution (essential for a long flat pulse), the beam waist must be well below the pixel dimensions.

Taking the output pulse as a function of different beam waists, we ended up with a beam waist of $w_0 = 20\,\mu m$ [7]. This value seems feasible for the chosen focal length and the foreseen input spot size. The beam waist w_0 after simple calculations is

$$w_0 = \frac{cos\,\theta_i}{cos\,\theta_d} \cdot \frac{\lambda\,f}{\pi\,w_{in}} \tag{21}$$

where w_{in} is the waist of the input beam at the grating. Having fixed all the parameters but the input waist, this w_{in} is 5.8 mm.

As for the choice of the spectral bandwidth $\Delta\omega$, note that the frequency interval $\Delta\omega$ is relevant to the rise time and plateau roughness of the rectangular pulse and also to the shaper dimensions. The bandwidth of $30\,\pi$ rad/ps comes from a trade-off among the three requirements of fast rise time, flat plateau and reduced mechanical dimensions.

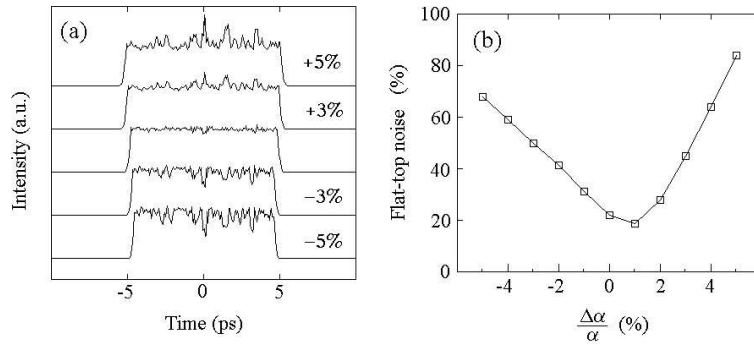## 8.1 The stability of operation as function of paramter's perturbation

Figure 26: (a) Variation of the signal plateau flatness at the third harmonic for different values of $\Delta\alpha/\alpha$. (b) A 20 % enhancement of the plateau roughness occurs for an angular dispersion variation of about 2 %. The flat-top noise was calculated by $(I_{max} - I_{min})/I_{average}$.
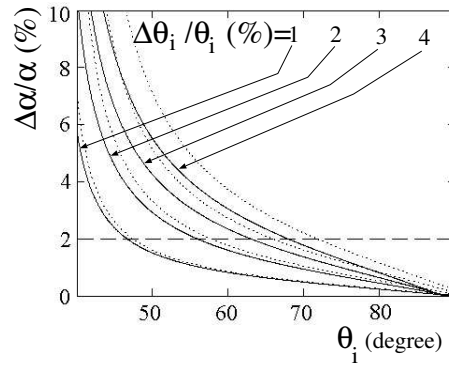
Figure 27: Sensitivity of dispersion α versus input angle θ_i at a fixed focal length of 700 mm. Continuous lines: percentage variations of 4, 3, 2 and 1% respectively. Dotted lines: negative variations in θ_i. Note that $\Delta\alpha/\alpha$ is not symmetric with respect to the two side variations and also that $\Delta\alpha/\alpha > 0$ when $\Delta\theta_i < 0$ and vice versa.

We investigated via simulations the system sensitivity to variations in the input pulse length, the dispersion (incident angle) and the input pulse profile. The sensitivity of the shaper to perturbations depends on the spectral acceptance, once the type of modulation has been fixed. In fact, we verified that the wider the spectral acceptance, the higher the system sensitivity to any variation, but also the smoother the pulse flatness at the optimized filter pattern. A pulse lengthening of a couple of femtoseconds leads to a 10% increase in roughness. It could be advisable to

choose a smaller portion of the spectral bandwidth and, hence, accept a lower flatness in order to obtain a lower sensitivity to pulse-length deviations. The increase in plateau roughness because of perturbation of the spatial dispersion (due to the variation in the incident angle) is shown in Fig. 26: its variation with $\Delta\alpha/\alpha$ is slow. The reason for the output change is that a variation in α produces a variation in the spectral components hitting the mask pixels. This leads to a spectral phase pattern that is no longer optimized for a flat output.

It is apparent from Fig. 26b that, accepting an enhancement of the roughness of up to 30%, the acceptable extent of the α variation is 2%. Note that the variation is not left-right symmetric about the centre. The parametric curves reported in Fig.27 present the percentage variation of α at the different input angles. The parameter of the curves is the percentage variation of the input angle as indicated in the figure. The line $\Delta\alpha/\alpha = 2\%$ shows that the allowed variation of the input angle is about 2% at the chosen $\theta_i \simeq 63^o$. This perturbation of the input angle can be easily controlled in an optic system.

To round off, we also performed simulations with the iterative Fourier transform (Gerchberg-Saxton) algorithm [12]. The simulated signal-output was notably worse than that obtained with our program based on the genetic algorithm.

9 A new concept of shaper for long laser target waveforms

We report here the article "A shaper for providing long laser target waveforms" Nucl. Instrum. Meth. Phys. Res. A 538 (2005) 1-7, except for the abstract and introduction.

Long rectangular pulses required by rf-guns indicate that the shaping system must both greatly enlarge the laser pulses and transform them from Gaussian-like to rectangular form. The shaping system we present here is tailored for long pulses generation. Its operation is based on an amplitude spectral modulation, made by the so-called 4f-system, followed by a linear space dispersion made by 2-grating stretcher (2g-stretcher). Our shaping problem is conveniently separated into a) the transformation of a short pulse into a long pulse and b) the transformation of a Gaussian form into a target form. The first task can be obtained by a 2g-stretcher which does a linear dispersion of the pulse spectral components. In fact, it provides a linear delay time among the spectral components

$$\tau(\omega) = \alpha\,\omega \qquad \text{referred to the central frequency } \omega_0 \qquad (22)$$

thus obtaining the spectral phase function

$$\phi(\omega) = \int_0^\omega \tau(\omega')d\omega' = \frac{1}{2}\alpha\omega^2. \qquad (23)$$

The latter task implies a proper spectral amplitude modulation. In mathematical terms an operator $H(\omega)$ has to act on the input amplitude spectral function $A_i(\omega)$ in such a way to get the wanted output spectral function $A_o(\omega)$

$$A_o(\omega) = H(\omega)A_i(\omega) \qquad (24)$$

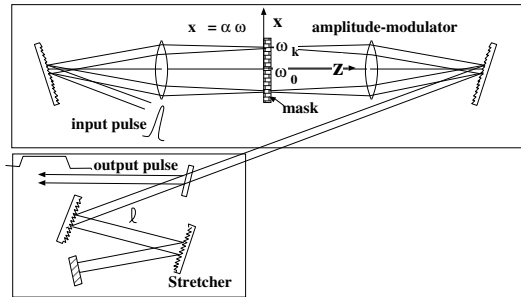Therefore, we must add a proper amplitude modulator to the 2g-stretcher. The shaping apparatus

Figure 28: Sketch of the new shaping system for long pulses. The amplitude modulator sub-part is a 4f-system, the second sub-part is the usual 2-grating apparatus for a linear time delay of the spectral components.

we are proposing consists of a 4f-system followed by a pair of diffraction gratings as shown in Fig. 28. The 4f-system, arranged in the configuration known as "zero dispersion pulse compressor", has the shaping mask at the focal plane [3] (center plane of the system) programmed as an amplitude modulator. The grating pair is set in a dispersive configuration so to behave as a stretcher with a linear time delay of the pulse spectral components. We call this shaper, composed with the two items, 4f-2g-system. The amplitude and phase modulations are decoupled from one another, as are Eqs. (22) and (24). The amplitude modulating function $H(\omega)$ in Eq. (24) is called filtering function.

9.1 The operation of a 4f-system as amplitude modulator

The operation of a 4f-system is described in details in reference [5]. Briefly, the spectral components of a pulse are first individually focused at the mask pixels, see Fig. 11, and then filtered according

to the mask filtering function $H(\omega)$. The spectral focalization (by a lens) in connection with the insertion within the system of a proper mode filter select out of the mask the lowest TEM_{00} mode [3, 13]. Hence, the filter function has the following expression

$$H(\omega) = \sqrt{\frac{2}{\pi\,w_0^2}} \int_{mask} M(x)\, e^{-2\,\frac{(x-\beta\omega)^2}{w_0^2}}\, dx \qquad (25)$$

Here w_0 is the beam waist of the focused beam at the masking plane (typically 20-100 μm), $M(x)$ is the physical masking function and β is the spatial dispersion of the pulse spectral components introduced by the grating coupled with the lens, that is $x(\omega) = \beta\,\omega$.

When w_0 is less than the pixel dimension Δx, the following approximation holds [3]

$$H(\omega) \sim M[x(\omega)] \qquad (26)$$

that is the filtering function $H(\omega)$ is equal to the physical function M(x) of the mask. We choose this operating condition for our system.

The output intensity $I_o(t)$ is found by performing the inverse Fourier transform

$$I_o(t) = \left| \int H(\omega)A_i(\omega)\, e^{i\,\frac{\alpha}{2}\omega^2}\, e^{-i\,\omega t}\, d\omega \right|^2 \qquad (27)$$

When the output pulse length is much longer than the input pulse length, which means a large α, the integral in Eq. (27) can be written as

$$I_o(t) \approx \{H[\omega(t)]A_i[\omega(t)]\}^2 = \tilde{I}_o[\omega(t)] \qquad (28)$$

where $\omega(t) = t/\alpha$. We observe that the two functions $H(\omega)$ and $A_i(\omega)$ are real. From this Eq. (28) we get that the temporal profile of the pulse $I_o(t)$ is equal to the power spectrum $\tilde{I}_o(\omega)$ profile. We can see that the stretcher simply transfers the spectral amplitude profile into the temporal amplitude profile. This occurs because a 2g-stretcher establishes a linear relation between frequency and time.
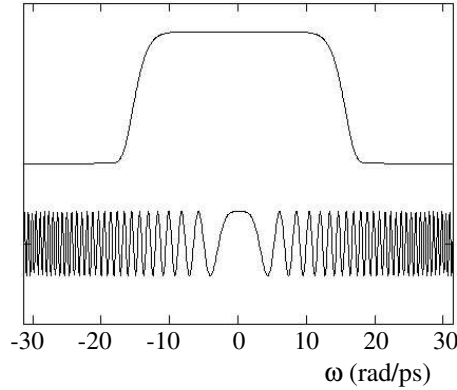

Figure 29: The upper curve is the output spectral amplitude $A_o(\omega)$, the lower curve is the $RE\{exp[i\,(\alpha/2)\omega^2 - i\omega t]\}$ function. the fast oscillating behavior of this second curve everywhere but the center explains the non-null contribution to the integral (27) only at the center coordinate t/α.

The result of Eq. (28) can be understood observing that the term $exp[i\,(\alpha/2)\omega^2 - i\omega t]$ of Eq. (27) is fast oscillating when ω is far from the value t/α, it is, instead, relatively smooth around t/α, see Fig. 29. Thus, that term operates, in a certain sense, as a $\delta(\omega - t/\alpha)$ function. This holds when $A_o(\omega)$ is smooth enough compared with that exponential term. In fact, the integral where the function is fast oscillating is near zero. This implies a short input pulse (i.e. wide $A_o(\omega)$) and a long output pulse (i.e. large α).

9.2 Some useful cases and sensitivity considerations

We discuss some practical cases with the aim of gaining a deeper insight into the physics of the 4f-2g-shaping-system. From Eq. (28) the filtering function turns out to be

$$H(\omega) = \frac{\sqrt{\tilde{I}_o(\omega)}}{A_i(\omega)} = \frac{A_o(\omega)}{A_i(\omega)}. \tag{29}$$

The equation suggests that the equality of $\tilde{I}_o(\omega)$ (the target spectral intensity profile) with $I_o(t)$
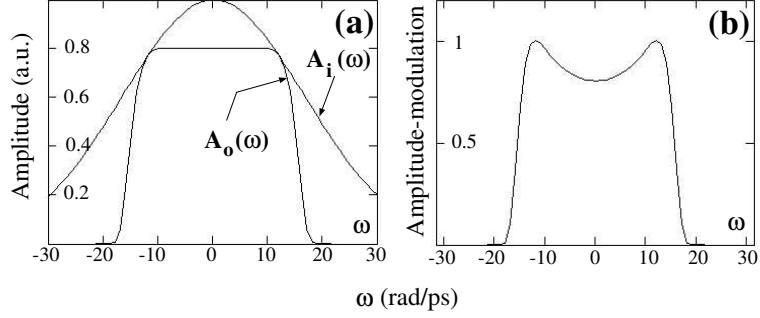

Figure 30: Left frame shows the input $A_i(\omega)$ (upper curve) and the output $A_o(\omega)$ (inside curve) spectrum amplitudes. $A_i(\omega)$ is a 100 fs wide Gaussian curve and $A_o(\omega)$ has the expression $A_o(\omega) = B\,exp(-(\omega/\gamma)^n)$ with n=12 (which means fast rise time). B and γ parameters are chosen to minimize the energy loss. The right frame shows the relative filter function $H(\omega)$.
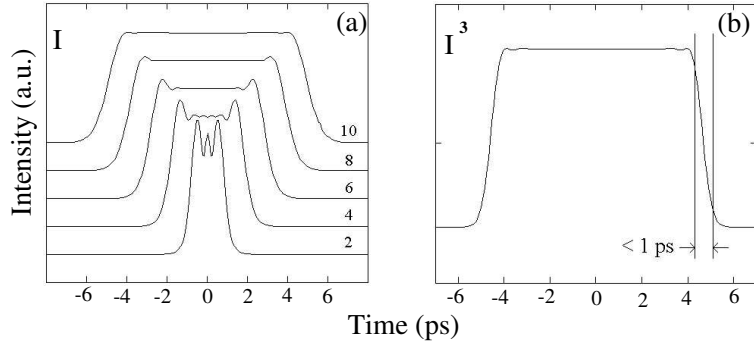

Figure 31: Left frame depicts the set of output pulses obtained through Eq. (27) with the $A_o(\omega)$ of the previous figure and with different arrangements of the stretcher so to get the pulse durations marked in the curves ($\Delta t = 10 - 2\ ps$). Right frame shows the 10 ps long pulse converted to the third harmonic. The rise time (from 10 % to 90 % of the total pulse height) is less than 1 ps.

(the target temporal intensity) implies to design this target profile inside the spatial frequency spectrum $A_i(\omega)$ curve. We start considering a rectangular target pulse (important for rf-guns) and a transform limited Gaussian input pulse with spectral amplitude $A_i(\omega)$. The Fourier spectrum in frequency of both the input and output signals is depicted in Fig. 30 left frame. In looking for an Δt wide pulse out from the stretcher, the relative α parameter after Eq. (22), must be

$$\alpha = \frac{\Delta t}{\Delta \omega}. \tag{30}$$

Here $\Delta \omega$ is the $A_o(\omega)$ bandwidth as shown in Fig. 30. Five numerically calculated signals out from the stretcher arranged for having lengths in the interval 2-10 ps (the input signal is the one

of Fig. 30) are shown in Fig. 31. We see that the pulse must be longer than 6 ps for having a good flat top. The third harmonic profile is caculated through the cube intensity I^3 of the fundamental. We tested that the six-power field $E(t)^6 = [A\cos[\omega t - \phi(t)]]^6$ did not have important envelope fluctuations during the pulse timewidth. We see from the figure that the rise time is less than 1 ps, as required by a class of rf-guns [1].
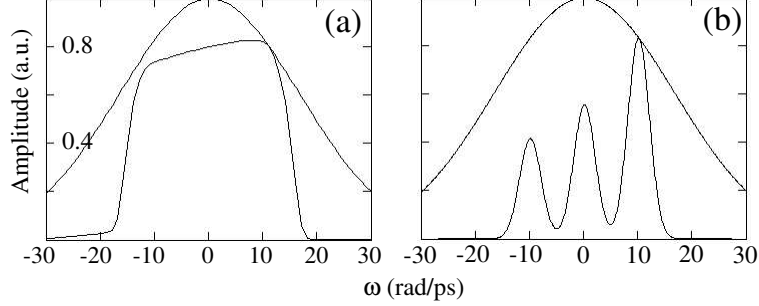

Figure 32: The figure shows both the input $A_i(\omega)$ and the output $A_o(\omega)$ amplitude spectra (with the Gaussian input pulse) for generating a ramp pulse, frame (a), and a train of three pulses, frame (b), as shown in the next Fig. 33.
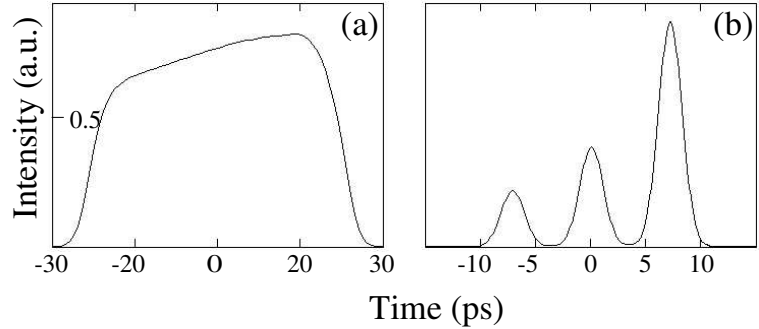

Figure 33: The figure shows the two output pulses obtained with the amplitude modulation of Fig. 32.

We apply the procedure to the relevant case of the ramp pulse [14]. As a third example we report also the case of the generation of a sequence of three pulses, with the aim of showing the power of our shaping system. As done in the previous case we have to program a mask filtering function $M(\omega)$ leading the target $A_o(\omega)$ to be a ramp (in the first case) and the sequence of pulses (in the second case) inside the input Gaussian spectrum profile $A_i(\omega)$, see Fig. 32. Then, once chosen the value of the α parameter, we have to solve Eq. (27). The result is depicted in Fig. 33. We chose for this last case an α value such that the output pulse turns out to be as long as $30\,ps$, with the aim of showing that this shaping system can easily deliver long pulses.

We must remark here that the amplitude modulating mask in laser systems with amplifiers and harmonic generators should be programmable with the aim at compensating the distortions introduced into the pulse by the non-linearities of the amplification and harmonic generation processes. This is the reason of the proposal of the 4f-system with a liquid crystal programmable spatial light modulator (LCP-SLM) in conjunction with a stretcher. The LCP-SLM device can be replaced by an optical window with the transmissivity profile found with the above LCP-SLM device, that is a transmission optical element tailored to the specific laser system. The transmissivity will have a super Gaussian profile with the modifications proper for recovering the distortions introduced in the amplification and frequency conversion processes.
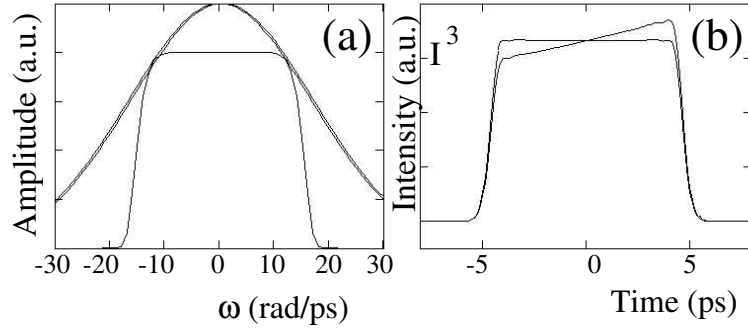
Figure 34: In left frame (a) the two spectral pulses shifted one another of 0.15 nm are depicted. Inside the input spectrum $A_i(\omega)$ the output spectral amplitude $A_o(\omega)$ is shown. The change of the output intensity waveform (at the third harmonic) due to the central frequency shift is shown in the frame (b). The amplitude percentage variation results about 20%.

A couple of considerations about the system sensitivity to perturbations are worth doing. One is that the 2f-2g-system is relatively insensitive to parameter perturbations. We observe, incidentally, that it is easy to calculate the effect of the input pulse variations. In fact, once known $H(\omega)$, for a given modified input $A_m(\omega)$ the output intensity pulse is simply $I_m(\omega(t)) = (H(\omega(t))A_m(\omega(t)))^2$. The change of the output signal profile because of a $0.15\,nm$ shift of the central frequency of the laser pulse (a value roughly estimated as possible in Ti:Sa laser) is smooth, as shown in Fig. 34. The correspondent variation $(I_{max} - I_{min})/I_{average}$ at the third harmonic is about 20%. This variation is four times less than that obtained with a 4f-system with phase-only-modulation [7]. The sensitivity of the system is reduced by minimizing the spectral interval $\Delta\omega$ selected for the output pulse. We notice that the filtering function will be reprogrammed in the laser operation on the base of the deformations observed experimentally on the output pulse.
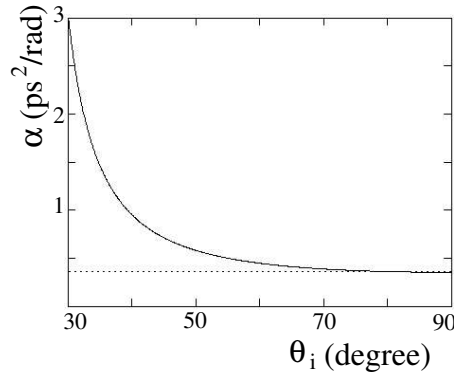
Figure 35: The figure shows the behavior of the parameter α as function of the input angle having set the distance between the two gratings $\ell = 5\,cm$ and the period of the gratings 1740 grooves/mm. The dotted line indicates the values which must have the parameter α in order to get a a pulse length of 10 ps assuming 10 nm of frequency interval.

A second consideration is addressed to the perturbation of the input angle θ_i into the stretcher. From the expression of the dispersive coefficient

$$\alpha = \frac{\lambda_0^3 \ell}{\pi c^2 d^2} \left[1 - \left(\frac{\lambda_0}{d} - sin\,\theta_i \right)^2 \right]^{3/2} \tag{31}$$

graphically shown in Fig. 35, we can figure out that choosing a configuration with an input angle

greater than fifty degrees the stretcher is practically insensitive to input angle θ_i perturbations. In the above equation λ_0 is the central wavelength, ℓ is the distance of the two gratings (as shown in Fig. 28), c is the speed of light and d is the grating period. We notice that a large input angle in the stretcher means small non-linear terms in the dispersion, thus the delay time $\tau(\omega)$ is linear with frequency to a very good approximation.

9.3   Considerations

This new conceptual design of a shaping system tailored for relatively long target pulses is important for shaping the rectangular pulses to be applied to radiofrequency electron guns. Simulations show that the system is very efficient for the goal, having it a simple arrangement, a very low sensitivity to parameters perturbation and being it able to provide easily variable waveforms.

10 Pulse shaping at the second harmonic generation

We report here the article "Rectangular Pulse Formation in a Laser Harmonic Generation" Appl. Phys. B (2005) exept abstract and introduction.

In this section we investigate beam propagation and harmonic generation in the common KDP crystal, using a suitable numerical model. Moreover, we analyze and discuss the modification of the pulse profiles, both in time and frequency domain, on the base of a simplified and clarifying analytical theory. We conclude with some considerations about the experimental setup.

10.1 Beam propagation within a non-linear crystal: the model and the results

For the analysis of the nonlinear interaction leading to second harmonic generation in birefringent χ^2 media, we consider the propagation of quasi-monochromatic electromagnetic fields, with the electric components E_1 at the fundamental angular frequency ω_1 (the ordinary ray in our case), and E_2 at the harmonic frequency $\omega_2 = 2\omega_1$ (the extraordinary ray) written as

$$E_i(z,t) = A_i(z,t) \exp\left[i(k_i z - \omega_i t)\right] + c.c \;, \qquad (i = 1,2), \qquad (32)$$

where A_i are complex amplitudes, k_i are the corresponding wave vectors, z is the propagation axis. We neglect the transverse variation of the fields. In the framework of the slowly varying amplitude approximation, the interaction between co-propagating fields can be described by the coupled differential equations [16]

$$
\begin{aligned}
\frac{\partial A_1}{\partial z} + \frac{1}{v_{g1}}\frac{\partial A_1}{\partial t} &= i\frac{2\omega_1\, d_{eff}}{c\, n_1}\, A_2\, A_1^*\, e^{i\Delta k\, z} \\
\frac{\partial A_2}{\partial z} + \frac{1}{v_{g2}}\frac{\partial A_2}{\partial t} &= i\frac{\omega_2\, d_{eff}}{c\, n_2}\, A_1^2\, e^{-i\Delta k\, z}
\end{aligned}
\qquad (33)
$$

where v_{gi} and n_i are the group velocity and the refraction index relative to the field E_i, d_{eff} is the effective second order susceptibility, and $\Delta k = k_2 - 2 k_1$ is the phase mismatch. The proper value of d_{eff} is determined by the angles χ and ϕ defining the propagation direction with respect to the principal optical axis of the selected material. The propagation direction is determined by the condition of maximum interaction efficiency, which corresponds to the condition of perfect phase matching $\Delta k = 0$ [17]. On the other hand, the values of the group velocities and refraction indexes depend on the propagation direction and are calculated by the so-called Sellmeier dispersion equations [18]. In this model we retain the effect of group velocity differences (*i.e.* the temporal walk-off), but neglect the group velocity dispersion, which has effect only for pulse durations well below the ps of our interest [19]. We do not consider, in addition, the effects of higher nonlinearities, which introduce a small phase mismatch and turn out to be relevant only for very energetic short pulses [20, 21]. The spatial walk-off due to the small angle between the directions of energy flux and wave vector within the extraordinary ray of birefringent crystals is neglected under the assumption of a broad transverse area of the pulse.

The coupled equations (33) are used to numerically calculate the second harmonic pulse emerging from the non-linear crystal at $z = L$, being L the crystal length. The complex field amplitudes at $z = 0$ are respectively $A_1(0,t)$ for the first harmonic and $A_2(0,t) = 0$ for the second harmonic. $A_1(0,t)$ represents the envelope of the incident pulse at fundamental frequency. It will have a profile suitable for obtaining the target profile after the interaction, and is created by a shaper. A brief description of the numerical method, which has a global second order accuracy, is given in the Appendix. In all the simulations we have selected for definiteness the condition of perfect phase matching $\Delta k = 0$, which guarantees the minimum deformation of the pulses during the interaction.

With the aim of generating a harmonic rectangular pulse of 10 ps, we take into consideration as input pulses for the up-conversion within the non-linear crystal, the two pulses generated by the shaper of Fig 28. The source laser pulse entering the shapers is assumed to have a Gaussian-like

profile with a time FWHM of 100 fs, that is a bandwidth of about 500 GHz. This relatively wide spectral bandwidth is necessary for creating a rectangular laser pulse with fast rise time.

The crystal considered for the harmonic generation is a KDP with a length $L = 500\mu$m, and the maximum intensity of the input signal is chosen below the threshold for damage (which depends on the temporal length of the pulse). The selected length turns out to be a good compromise between the second harmonic conversion efficiency and pulse profile maintenance, as shown by the shape of the output intensity $I_2 = 2\varepsilon_0 n_2^2 v_{g2} |A_2|^2$ of the up-converted pulses for different crystal lengths depicted in Fig. 36. The intensity profile of the second harmonic increases with the crystal length, but the top evolves from the flat to a hilled fashion. A simple theoretical explanation is discussed in the next section.
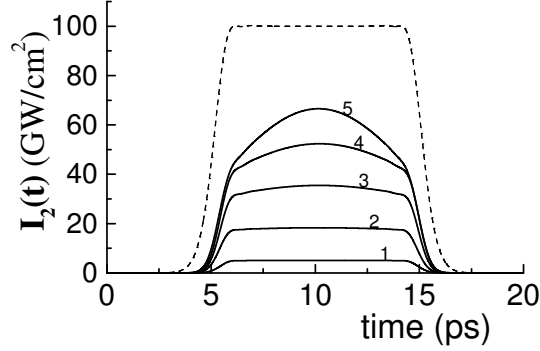
Figure 36: The graphs from 1 to 5 are the harmonic output pulses $I_2(t)$ obtained by Eqs. (33) for crystal lengths spanning the values 200-400-600-800-1000 μm, respectively. The dashed graph is the input signal intensity $I_1(t)$ obtained with the 4f-2g shaping system arranged for that target pulse.

Let us now consider the two shapers.
(1) *Input pulse generated by a 4f-2g shaper*
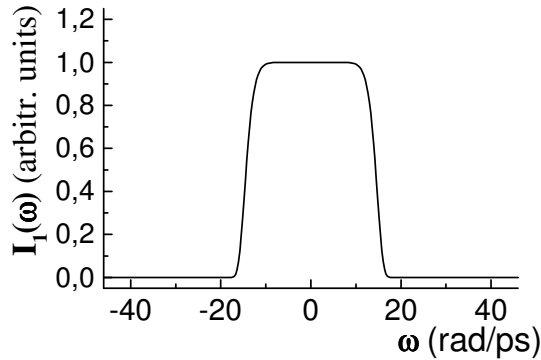
Figure 37: The picture depicts the spectral pulse profile performed by the spectral amplitude modulation. This laser pulse then enters the stretcher (second section of the shaping system) and afterwards enters the non-linear crystal for the second harmonic generation.

We consider first the 4f-2g-shaping system. The amplitude modulation performs a square profile of the pulse power spectrum as depicted in Fig.37. We have run the propagation equations with a set of five input pulses shaped with progressively increased temporal width up to 10 ps. Fig. 38 shows the second harmonic output pulses $I_2(t)$, central column, and the corresponding power spectra $I_2(\omega)$, right column. All the output pulses have the same 10 ps temporal length because the lacking length after the first un-complete stretching (before the SHG, second harmonic generation) is completed by a second stretcher set just after the SHG crystal. The maximum

intensity of the input signal profile $I_1(t)$ is selected to obtain near equal values for the intensity maxima of the output pulse, roughly following the simple rule $I_1(max) \times \sqrt{\Delta t} \approx const$, where Δt is the input pulse FWHM. These pictures show that a rectangular SHG target pulse can be accomplished only with suitable shaping and stretching of the input pulse, before entering the crystal. Moreover, the power spectrum profile in the right column result very similar to the temporal intensity profile for all the input different temporal pulses, in contrast with the behavior of the fundamental harmonic. This fact was discussed in [15], and is theoretically explained in the following section.
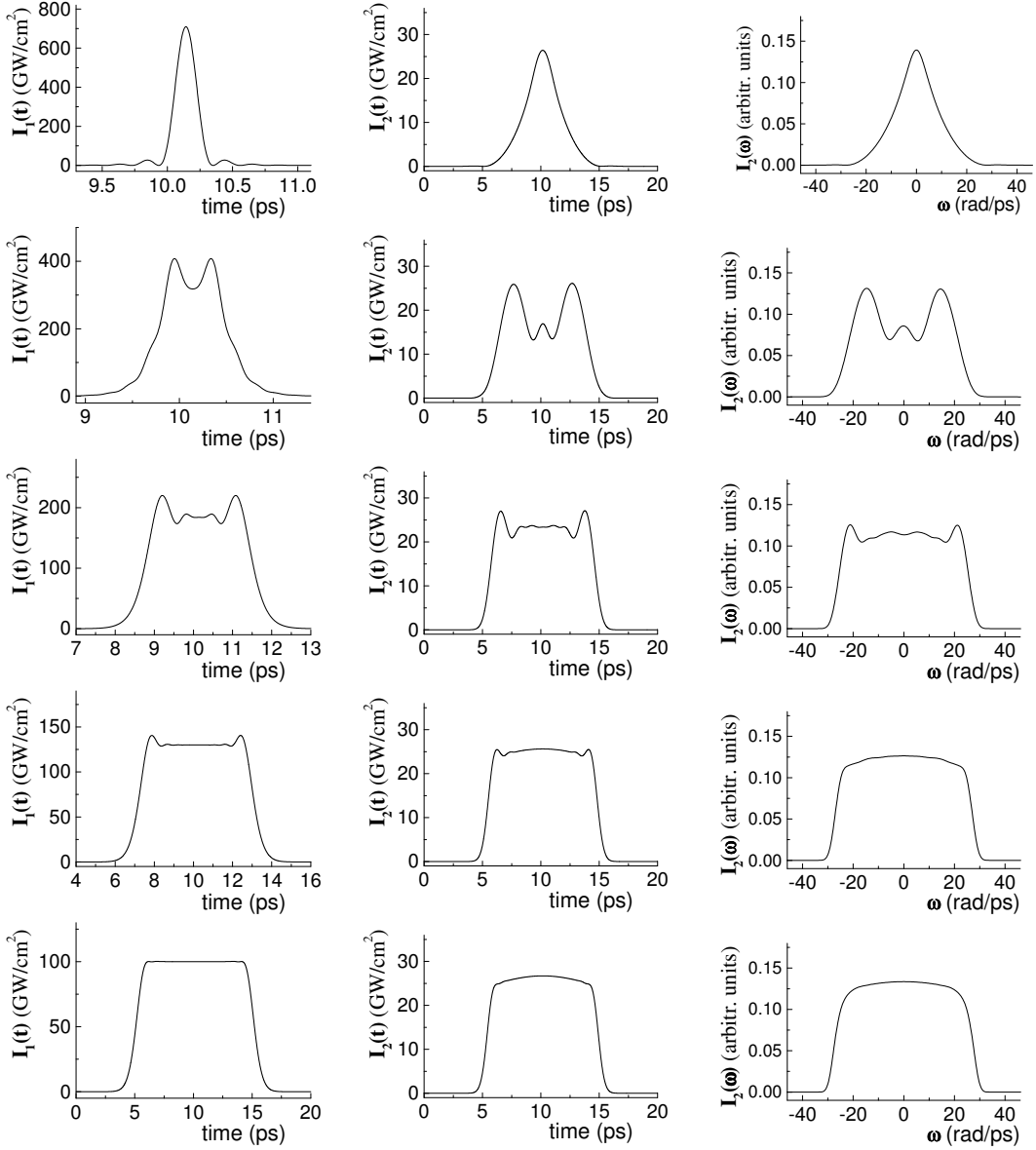
Figure 38: The left column shows the temporal profiles of the input pulses after spectral amplitude modulation and a partial chirping; the center column shows the temporal profiles of the output second harmonic pulses after completing the chirping up to 10 ps length; the right column shows the corresponding normalized power spectra.

(2) *Input pulse generated by a 4f-shaper with phase-only modulation*
We have run Eqs. (33) also with the input pulse obtained by a 4f-system whose mask is arranged

for obtaining a 10 ps pulse with phase-only modulation. The appropriate phase function $H(\omega) = exp[i\Phi(\omega)]$ is found by a numerical calculation via an adaptive algorithm. We have followed two different numerical approaches: in one the adaptive algorithm searches for the appropriate phase filter function patterned at the mask pixels which again provides at best the target profile [7]; in the second numerical approach we expanded the phase function in power series

$$\Phi(\omega) = a\,\omega^2 + b\,\omega^4 + c\,\omega^6 + \dots \tag{34}$$

and the adaptive algorithm searches the coefficients of the series for obtaining an output profile approaching at best the target one.

The output SHG pulses obtained by Eqs. (33) with the two phase functions found along the two lines of calculations are depicted in Fig. 39. The final pulses come out dramatically different in the two cases: the line of the power expansion leads to a fairly smoothed pulse, whereas the line of the direct calculation of the phase of the pixels leads to an output pulse profile flat on the average, but with a lot of superimposed fast spikes.
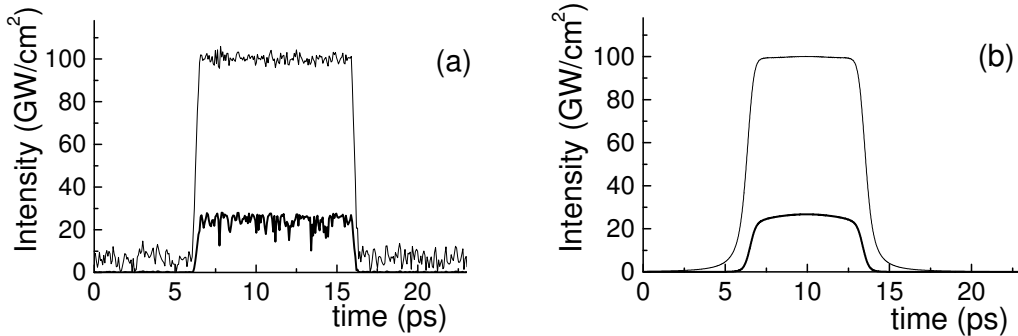

Figure 39: Frame (a): the upper curve is the input signal with a phase-only modulation calculated by an adaptive algorithm directly for the pattern of the mask pixels. The lower curve is the calculated second harmonic output after the interaction within the non-linear crystal. Frame (b): the upper curve is the temporal pulse profile shaped by a phase-only modulation calculated via the optimization of a power expansion coefficients of the phase function by an adaptive algorithm. The lower curve is the up-converted pulse.

10.2 A simplified theory of second harmonic generation with laser pulses with different profiles

In this section we present an approximated theoretical view, which leads to a simplified evolution equation for the second harmonic generated field. This equation allows a picture of the problem which enlightens the physics underlying the observed features of the SHG laser pulses.

Assuming low up-conversion efficiency in crossing the SHG crystal, we can neglect the right hand side in Eq. (33); therefore the slowly varying amplitude of the input pulse A_1 propagate along the crystal remaining practically undepleted. As a straightforward consequence, A_1 can be written as a function depending on the variable $t - z/v_{g1}$ only. The relevant propagation equation for the second harmonic slowly varying amplitude A_2 now reads

$$\frac{\partial A_2}{\partial z} + \frac{1}{v_{g2}}\frac{\partial A_2}{\partial t} = i\gamma\,[A_1(t - z/v_{g1})]^2\,e^{-i\Delta k\,z}\,, \tag{35}$$

having put $\omega_2\,d_{eff}/c\,n_2 = \gamma$. A more useful equation is obtained by changing the time frame of reference with $t' = t - z/v_{g2}$

$$\frac{\partial A_2}{\partial z} = i\gamma\,\left[A_1\left(t' + \frac{z}{v_{g2}} - \frac{z}{v_{g1}}\right)\right]^2\,e^{-i\Delta kz} \equiv i\gamma\,[A_1(t' + \beta z)]^2\,e^{-i\Delta kz}\,, \tag{36}$$

where $\beta = 1/v_{g2} - 1/v_{g1}$ is the group velocity mismatch parameter. In absence of this mismatch (*i.e.* $\beta = 0$) the solution of this equation at the end facet of the crystal is well known [17] and reads

$$A_2(L) = i\,\gamma\,A_1^2\,\frac{e^{-i\,\Delta k\,L}-1}{-i\,\Delta k}\,,\tag{37}$$

showing that $A_2(t) \propto A_1(t)^2$, and the maximum intensity of the second harmonic is obtained when the phase matching condition $\Delta k = 0$ is fulfilled. Assuming the validity of this condition for all the spectral components $\tilde{A}_2(\omega, z)$ of the generated light pulse, we may perform the transformation into the frequency domain of Eq. (36), obtaining

$$\frac{\partial \tilde{A}_2}{\partial z} = i\gamma\,e^{-i\,\beta z\omega}\,\tilde{A}_1(\omega) \otimes \tilde{A}_1(\omega)\,,\tag{38}$$

where $\tilde{A}_1(\omega)$ is the incident pulse in the frequency domain, and the symbol $\otimes$ indicates a convolution integral

$$\tilde{A}_1(\omega) \otimes \tilde{A}_1(\omega) = \int \tilde{A}_1(\omega')\,\tilde{A}_1(\omega - \omega')\,d\omega'\,.\tag{39}$$

Solving Eq. (38) with zero initial condition, we get the final expression

$$\tilde{A}_2(\omega, z) = i\,\gamma\,z\,\left(\frac{e^{-i\,\beta z\omega}-1}{-i\,\beta z\omega}\right)\cdot\tilde{A}_1(\omega) \otimes \tilde{A}_1(\omega)\,,\tag{40}$$

This equation (in the frequency domain) indicates that the up-converted pulse is given by the convolution of the input pulse with itself multiplied by a modulation factor.

It is now clear that the non-linear crystal will couple the spectral components of the input pulse at frequencies ω_i and ω_j satisfying the matching condition $\omega_i + \omega_j = \omega_{SHG}$. Therefore the observed intensity $I_2(\omega) \propto |\tilde{A}_2(\omega)|^2$ of the second harmonic will result from the contribution of all the input spectral components complying with the matching condition. The intensity is modulated by a factor $\texttt{sinc}^2(x)$, where $x = \beta z\omega/2$. This factor defines the frequency bandwidth over which the SHG intensity is significantly different from zero. The bandwidth is progressively reduced with the crystal length as shown in Fig. 40 by the graphs of the quantity $C_N = I_2(\omega)/L^2$
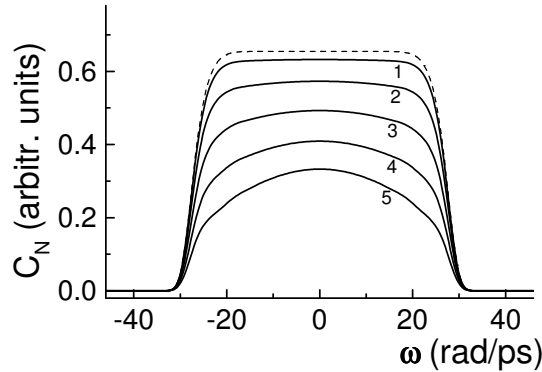
Figure 40: Profiles of the quantity C_N in the frequency domain for a set of different crystal lengths spanning the values 200-400-600-800-1000 μm respectively, as in Fig. 36. The dashed line is the contribution of the convolution term.

(normalized power spectrum divided by length squared) versus the crystal length. The pulse profile evolves from flat to round with the increase of the crystal length L due to the fact that the flat entering pulse is convolved (see the discussion in the next paragraph) with a $\texttt{sinc}$ function in the interaction. Note that the spectral content of the output pulse is determined substantially by the $\texttt{sinc}$ function bandwidth as the crystal reaches the length of 1000 μm. This effect comes from

the higher losses at higher frequencies. This leads to the same rounding effect on the temporal profile, as shown in Fig. 36.

We analyze now the results obtained in the two cases of 4f-2g and 4f-systems on the base of previous considerations, at the fixed crystal length selected for keeping an appropriate frequency bandwidth.

(1) *Input pulse for SHG crystal generated by a 4f-2g shaper*

The pulse to be transformed is assumed to be a transform limited Gaussian pulse. A rectangular spectrum profile $A_1(\omega)$ (as depicted in Fig. 37) is generated by a proper amplitude modulation. When no chirp is applied the expected result of the convolution integral (39) is simply a simil-triangular shaped SHG pulse. This result is, in fact, obtained by the complete equation system (33) as shown by the first frame second row of Fig. 38.

Let us consider, then, the case with some chirping (that is with the phase modulation $\Phi(\omega) = (1/2)\,\alpha\,\omega^2$). The new amplitude $A_1(\omega)$ will assume the form

$$A_1(\omega) = S_1(\omega)\,e^{i\frac{1}{2}\alpha\,\omega^2} \tag{41}$$

where $S_1(\omega) = \sqrt{I_1(\omega)}$, with $I_1(\omega)$ the power spectrum of the first harmonic. The amplitude of the second harmonic in the frequency domain will have the expression (discarding the immaterial modulation factor)

$$A_2(\omega) \propto \int S_1(\omega')\,S_1(\omega - \omega')\,e^{i\frac{1}{2}\alpha[(\omega-\omega')^2+\omega'^2]}\,d\omega'\,. \tag{42}$$

The exponential function

$$e^{i\,\alpha(\frac{1}{2}\omega^2 - \omega\,\omega' + \omega'^2)} \tag{43}$$

is a fast oscillating function for all ω' except at the frequency coordinate $\omega' = \omega/2$; the larger is the coefficient α (that is the longer the stretching), the sooner starts the fast oscillation. Therefore, if α is large enough, the integral turns out to be near zero everywhere except at $\omega' = \omega/2$, *i.e.* that term operates as a δ-function. The integral (42) can be approximately written as

$$
\begin{aligned}
A_2(\omega) &\approx \int S_1(\omega')S_1(\omega-\omega')\,e^{i\,\alpha(\frac{1}{2}\omega^2 - \omega\,\omega' + \omega'^2)}\,\delta\left(\omega' - \frac{\omega}{2}\right)\,d\omega' \\
&\approx S_1^2\left(\frac{\omega}{2}\right)\,e^{i\,\alpha\,(\omega/2)^2}
\end{aligned} \tag{44}
$$

From this equation we deduce that the spectrum width of the second harmonic is two times larger than that of the first one, and that the spectral profile is similar (squared) to the profile of the first harmonic when the stretching is strong enough. These results reproduces almost exactly those obtained by the simulations with Eqs. (33) as depicted in the right column of Fig. 38. Furthermore, we observe that the delay times of the spectral components for the first and second harmonics are respectively

$$\tau_1(\omega) = \frac{d\Phi_1}{d\omega} = \alpha\,\omega \qquad\qquad \tau_2(\omega) = \frac{d\Phi_2}{d\omega} = \frac{1}{2}\,\alpha\,\omega\,. \tag{45}$$

This result comply with the fact that the temporal width of the second harmonic tends to be the same as the temporal width of the completed stretched first harmonic, as one can see in Fig. 38.

(2) *Input pulse generated by a 4f-shaper with phase-only modulation*

We must consider only the case of the input pulse formed by the phase function obtained by a power expansion. The pulse entering the crystal is already fairly shaped. From the mathematical point of view we have to treat again with a convolution integral of the type (44), with the exponential phase function even faster oscillating than that considered in the first shaper with a simple chirping. Therefore, the conclusion outlined above is immediate. Incidentally, we could end up straightforward to this conclusion observing that, being the input pulse already formed, we could directly exploit Eq. (37) in the temporal domain.

10.3 Some experimental considerations

The response function for the generation of a target pulse comes out as numerical solution via an adaptive algorithm. This solution is implemented in the laser system by a proper setting of the shaping system. A computer, running the adaptive algorithm, can drive the system towards the right optical configuration of the shaper, being it inserted in a feedback loop between the output of the harmonic generator and the shaping system. In this configuration the detected output pulse is sent to the computer as input set of data and compared with the target pulse in terms of a cost function [7] and then the shaping system configuration is updated.

However, the operation of the laser system in relation to the pulse profile (provided with the shaper) is very sensitive to mechanical and optical perturbations [7]. Since perturbations (in a large laser system) are un-avoidable, and since a shaping system is capable of bringing off the requested profile counter-reacting to perturbations with a proper re-setting, the laser system must be arranged in an selfcontrolled configuration. The output pulse is continuously measured, sent to a computer for comparison with the target pulse and the computer drives the shaping system to the right spectral amplitude and/or phase re-modulation (depending on the shaping system type): the operational stability implies an adaptive behavior.

In connection with the operation of measuring the output pulse profile and with the operation of computer-assisted setting of the shaping system, we remark that: the detection of a spectrum by a spectrum analyzer is immediate, whereas the detection of a temporal pulse is complicate and difficult. This later operation is customary done by a cross-correlation. In our system the cross-correlation technique cannot be exploited because of the 10 Hz repetition rate. In fact, this low repetition rate leads to a system resetting time of about half an hour. About the technique of the single-shot autocorrelation, we observe that, even if it would be enough fast, for extracting the temporal profile from the autocorrelation graph a numerical de-correlation calculation must be done, and, this calculation needs also a spectrum measurement [23]. These considerations lead to conclude that a 4f-2g shaping system allows an easier handling because a system re-setting is done (i) by measuring the spectrum of output pulse at each shot and (ii) by connecting the spectrum data to a computer which does the rest (that is compares the output and the target profiles (in our case of 10 ps the profile of the last figure in center column in Fig. 38) and organizes the proper spectral variations).

10.4 Considerations

A relatively long and powerful second harmonic laser pulse, efficiently generated trough the inter-action within a non-linear crystal, has a rectangular temporal profile only if the profile of the input pulse is properly designed. The production of a proper input pulse requires the implementation in a laser system of a shaping system capable of giving to laser pulses (via spectral amplitude and/or phase modulation) profiles of smooth rectangular-swallow-tailed forms.

Appendix

Eqs (33) are conveniently solved with a second order finite difference scheme, appropriate for studies on laser pulse propagation [22]. We first define dimensionless complex amplitudes with

$$C_1 = A_1 e^{-i\Delta kz/2} \sqrt{\frac{2\varepsilon_0 n_1 c}{I_0}} \; ; \qquad\qquad C_2 = A_2 \sqrt{\frac{2\varepsilon_0 n_2 c}{I_0}} \qquad (46)$$

where I_0 is a reference intensity, usually coincident with the maximum of the incident pulse. By changing the independent variables with the relations

$$\tilde{t} = \left(t - \frac{z}{v_{g1}}\right)\left(\frac{1}{v_{g2}} - \frac{1}{v_{g1}}\right)^{-1} \; ; \qquad\qquad \tilde{z} = z \qquad (47)$$

we get the reduced system of equations

$$\frac{\partial C_1}{\partial \tilde{z}} = i\alpha\, C_2 C_1^* - i\frac{\Delta k}{2} C_1 \qquad (48)$$

$$\frac{\partial C_2}{\partial \tilde{z}} + \frac{\partial C_2}{\partial \tilde{t}} = i\alpha\, C_1^2$$

where

$$\alpha = \omega_1 d_{eff} \sqrt{\frac{2I_0}{\varepsilon_0 c^3 n_2 n_1^2}} \;. \qquad (49)$$

The finite difference scheme is obtained by dividing the $\tilde{z} - \tilde{t}$ plane into a grid with spacing $\Delta\tilde{z} = \Delta\tilde{t}$, and making a second order Taylor expansion of $C_1(\tilde{z}, \tilde{t}), C_2(\tilde{z}, \tilde{t})$ about the grid points (m, n); the second derivatives are calculated by differentiating the Eqs. 48 and substituting a first order difference approximation for the simple derivatives. Therefore we obtain iterative expressions giving the amplitudes at time advanced grid points $C_i(m, n+1)$ as functions of the preceding time and space values $C_i(m-1, n+1), C_i(m, n)$ and $C_i(m-1, n)$. This procedure is numerically stable and has an overall truncation error of order $(\Delta\tilde{t})^2$.

11   Conclusions

The relatively low-cost medium technology laser system built in the LAB has demonstrated to be a good light source for research and development of shaping techniques. With it we tested the generation of many pulse profiles and developed the relevant computer programs for driving the shaping system as well as we could test the arrangements for optimized operations.

The up-grading of the laser source for the generation of dozen picosecond pulses is under progress. The goal is pursued through the implementation in the oscillator of a SESAM [9] (semiconductor saturable absorber). The foreseen pulse length of about 40 ps, instead of the to-day 80 ps, would allow to increase of, at least, a factor four the spectral bandwidth of the pulse with respect to the present bandwidth of 3 nm. The new feature of the light source will allow to do tests on picosecond rise times of rectangular pulses. In addition, the cross correlation diagnostic would become feasible.

We did the follwing tasks relevant for our JRA2-WP3:

1. the software based on a genetic algorithm governing the waveforms' generation within a laser system;

2. the design of the shaper based on a LC-SLM for the SPARC project;

3. the study of the sensitivity of the shaper to the perturbations of the laser sytem parametrs;

4. the proposal of a shaper of new concept for the generation of long target waveforms;

5. the analysis of the non-linear action on a rectangular pulse profile in the second harmonic generation;

6. the experimental tests of a laser system complete of a LC-SLM shaper generationg many waveforms.

References

[1] SPARC "Conceptual design of a high-brightness linac for soft X-ray SASE FEL source," EPAC 2002 (La Villette, Paris) 5 June 2002.

[2] J. Yang, F. Sakai, T. Yanagida, M. Yorozu, Y. Okada, K. Takasago, A. Endo, A. Yada, and M. Washio, J. Appl. Phys. **92,** 1608–1612 (2002).

[3] A. M. Weiner, Rev. Sci. Instrum., **71,** 1929-1960 (2000).

[4] P. Tournois, Opt. Commun. **140,** 245–249 (1997).

[5] S. Cialdi, I. Boscolo, *A laser pulse shaper for the low emittance radiofrequency SPARC electron gun*, report INFN-BE-03-3, Nucl. Instrum. Meth. Phys. Res. **526** (2004) 239-248.

[6] J.W. Nicholson, J. Jasapara, W. Rudolph, F.G. Omenetto and A.J. Taylor *Full-field characterization of femtosecond pulses by spectrum and cross-correlation measurements*, Opt. Lett. **24**, 1774-1776 (1999).

[7] S. Cialdi, I. Boscolo and A. Flacco, J. Opt. Soc. Am. **21**, 1693-1698 (2004).

[8] A.M. Weiner and D.E. Leaird, Opt. Lett. **15**, 51-53 (1990).

[9] C. Honninger, R. Paschotta, F. Mourier-Genoud, M. Moser and U. Keller, J. Opt. Soc. Am. B/**16**, 46-56 (1999).

[10] S. Backus, C. G. Durfee III, M. M. Murname and H. C. Kapteyn, Rev. Sci. Instrum. **69,** 1207–1223 (1998).

[11] W. Koechner, *Solid-State Laser Engineering* Springer.

[12] M. Hacker, G. Stobrawa and T. Feurer, Opt. Express **9**, 191 (2001).

[13] R. N.Thurston, J. P. Heritage, A. M. Weiner and W. J. Tomlinson, IEEE J. Quantum Electron, **22** (1986) 682.

[14] James Rosenzweig, UCLA, private communication

[15] S. Cialdi and I. Boscolo, Nucl. Insrtrum. Meth. Phys. Res. A 538, 1-7 (2005).

[16] Y.R. Shen, *The Principles of Nonlinear Optics*, Wiley, (New York, 1984)

[17] A. Yariv, *Quantum Electronics*, Wiley, (New York, 1989)

[18] A.V. Smith, SNLO nonlinear optics software, SANDIA National Labs. (http://www.sandia.gov/imrl/X1118/xxtal.htm)

[19] N.C. Kothari and X. Carlotti, J. Opt. Soc. Am. B **5**, 756-764 (1988).

[20] T. Ditmire, A.M. Rubenchik, D. Eimerl and M.D. Perry, J. Opt. Soc. Am. B **13**, 649-655 (1996).

[21] L.D. Noordam, H.J. Bakker, M.P. de Boer and H.B. van Linden van den Heuvel, Opt. Lett. **16**, 971 (1991).

[22] H.Risken and K.Nummedal, J. Appl. Phys. 39, 4662-4672, (1968).

[23] J.W. Nicholson, J. Jasapara, W. Rudolph, F.G. Omenetto and A.J. Taylor, Opt. Lett. **24** 1774-1776 (1999).